JOURNAL OF GEOPHYSICAL RESEARCH, VOL. 108, NO. B9, 2415, doi:10.1029/2003JB002411, 2003

Slope failure and volcanic spreading along the submarine south flank of Kilauea volcano, Hawaii

Julia K. Morgan
Department of Earth Science, Rice University, Houston, Texas, USA

Gregory F. Moore
Department of Geology and Geophysics, School of Ocean and Earth Science and Technology (SOEST), University of Hawaii, Honolulu, Hawaii, USA

David A. Clague
Monterey Bay Aquarium Research Institute, Moss Landing, California, USA

Received 19 January 2003; revised 22 April 2003; accepted 7 May 2003; published 5 September 2003.

[1] New multichannel reflection data and high-resolution bathymetry over the submarine slopes of Kilauea volcano provide evidence for current and prior landsliding, suggesting a dynamic interplay among slope failure, regrowth, and volcanic spreading. Disrupted strata along the upper reaches of Kilauea's flank denote a coherent slump, correlated with the active Hilina slump. The slump comprises mostly slope sediments, underlain by a detachment 3–5 km deep. Extension and subsidence along the upper flank is compensated by uplift and folding of the slump toe, which surfaces about midway down the submarine flank. Uplift of strata forming Papa'u seamount and offset of surface features along the western boundary of Kilauea indicate that the slump has been displaced ~3 km in a south-southeast direction. This trajectory matches coseismic and continuous ground displacements for the Hilina slump block on land, and contrasts with the southeast vergence of the rest of the creeping south flank. To the northeast, slope sediments are thinned and disrupted within a recessed region of the central flank, demonstrating catastrophic slope failure in the recent past. Debris from the collapsed flank was shed into the moat in front of Kilauea, building an extensive apron. Seaward sliding of Kilauea's flank offscraped these deposits to build an extensive frontal bench. A broad basin formed behind the bench and above the embayed flank. Uplift and back tilting of young basin fill indicate recent, and possibly ongoing, bench growth. The Hilina slump now impinges upon the frontal bench; this buttress may tend to reduce the likelihood of future catastrophic detachment. *INDEX TERMS:* 0930 Exploration Geophysics: Oceanic structures; 1824 Hydrology: Geomorphology (1625); 3022 Marine Geology and Geophysics: Marine sediments—processes and transport; 3025 Marine Geology and Geophysics: Marine seismics (0935); 8010 Structural Geology: Fractures and faults; *KEYWORDS:* Kilauea volcano, slope failure, landslides, volcanic spreading

Citation: Morgan, J. K., G. F. Moore, and D. A. Clague, Slope failure and volcanic spreading along the submarine south flank of Kilauea volcano, Hawaii, *J. Geophys. Res.*, *108*(B9), 2415, doi:10.1029/2003JB002411, 2003.

1. Introduction

[2] Large-scale landslides and debris avalanches are known to play an important role in the evolution of oceanic volcanoes around the world [e.g., *Wolfe et al.*, 1994; *Duffield et al.*, 1982; *Lènat et al.*, 1989; *Holcomb and Searle*, 1991; *Krastel et al.*, 2001; *Moore et al.*, 1994; *Watts and Masson*, 1995]. Volcanic landslides are closely linked with geologic hazards such as earthquakes, shoreline collapse or submergence, and destructive tsunamis that can impact widespread coastal communities [e.g., *Lipman et al.*, 1985; *Tilling et al.*, 1976; *Satake et al.*, 2002; *Day et al.*, 1999; *Ward*, 2002]. The relative infrequency of catastrophic submarine landslide events along volcano flanks means that none have been captured in the short historical record; their occurrence, origins, and resulting structural geometries are interpreted largely from surficial observations [e.g., *Moore et al.*, 1989; *Watts and Masson*, 1995]. New observations along the submarine flank of Kilauea volcano on Hawaii, currently the most active volcano on Earth, have now revealed the subsurface structure of an active submarine landslide and the remnants of an ancient landslide. The results of our study define the sequence of events responsible for the present-day configuration and behavior of the active volcano, which reflect a complicated interplay of volcanic processes that may be preserved or repeated at many other oceanic volcanoes.

0148-0227/03/2003JB002411$09.00

[3] The Hilina slump is an active landslide that breaks the mobile southeast flank of Kilauea volcano and is headed on land by a system of seaward facing normal faults, the Hilina fault system (Figure 1). Major rupture and offset occurred along these faults as recently as 1975, during the *M*7.2 Kalapana earthquake that struck the south coast of Hawaii beneath Kilauea's south flank. Coincident with this event, a large region seaward of the fault zone subsided and slipped about 8 m seaward, defining the subaerial portion of the largely submarine, active slump block [*Lipman et al.*, 1985]. The offshore extent and geometry of the Hilina slump is not known. It may be a deep-seated structure, encompassing much of the south flank of Kilauea [*Lipman et al.*, 1985; *Moore et al.*, 1989, 1994], or alternatively, a thin, surficial body restricted to the upper slope strata blanketing the submarine flank [*Swanson et al.*, 1976]. These two end-member interpretations have very different implications for the stability of the Hilina slump and the potential for catastrophic detachment, as has occurred elsewhere in the islands [e.g., *Moore et al.*, 1989].

[4] In recent years, several marine geophysical, mapping, and sampling surveys have been carried out over Kilauea's south flank, serving to clarify the slump geometry and deformation history of the flank. In this study, we focus on two surveys conducted in 1998 over the upper northwestern region of the flank to evaluate submarine evidence for slumping along the flank. A multichannel seismic (MCS) survey carried out on board the R/V *Maurice Ewing* surveyed the western boundary region and the Halape shoreline reentrant of Kilauea's upper flank (Figure 1). Subsequently, a new high-resolution bathymetric survey using a SIMRAD EM300 system [e.g., *Clague et al.*, 1998; *MBARI Mapping Team*, 2001] was conducted over a structural high known as Papa'u seamount along Kilauea flank's western boundary (boxed, in Figure 1).

[5] The new data indicate that the active Hilina slump is a shallow feature encompassing Papa'u seamount, and restricted to the upper, northwestern portion of the mobile flank. Buried evidence of thinned and disrupted slope strata to the east of the slump reveals that the south flank experienced a major, catastrophic failure in the recent past, possibly resulting from the breakup of a much larger proto-Hilina slump. Subsequently, seaward sliding of the south flank offscraped the scattered landslide debris to form a broad frontal bench, which now buttresses the downslope motion of the remnant Hilina slump. This complicated sequence of slumping, slope collapse, and gravitationally driven volcanic sliding defines a model that may be repeated along the flanks of oceanic volcanoes around the world.

2. Hilina Slump and Kilauea's South Flank

[6] The broad shield of Kilauea volcano was built upon the flank of Mauna Loa volcano along the southeast island of Hawaii; the exact boundary between the two volcanoes is poorly defined. Two rift zones radiating from Kilauea's summit define the eruptive locus of the volcano (Figure 1); the active east rift zone (ERZ) extends nearly 50 km on land and continues offshore an additional 70 km as the Puna ridge and the southwest rift zone (SWRZ) is morphologically subdued and less active due to the buttressing effect of Mauna Loa. Kilauea's south flank, the tectonic domain embraced by the two rift zones, is cut by a set of arcuate, seaward dipping normal faults, the Hilina fault zone (Figure 1), interpreted to mark the head of a large submarine landslide, the Hilina slump [e.g., *Stearns and Clark*, 1930; *Moore and Krivoy*, 1964; *Swanson et al.*, 1976; *Lipman et al.*, 1985; *Smith et al.*, 1999]. Cumulative fault scarp relief of ~800 m near the center of the fault system yields a minimum offset along the Hilina fault system [*Lipman et al.*, 1985], as ponded, postoffset lava flows mask the true displacement of the downdropped blocks [e.g., *Swanson et al.*, 1976]. Ash units dated to ~49 ka, exposed along the fault scarps, provide a minimum age for fault activity [*Clague et al.*, 1995]. The Hilina fault scarps lose relief to the southwest and northeast where they have been progressively buried by younger lava flows (Figure 1).

[7] The Hilina slump is active today and subject to coseismic displacements [e.g., *Lipman et al.*, 1985] and aseismic slip events, as recently captured along the Hilina detachment following a major rainfall event [*Cervelli et al.*, 2002]. The last two great earthquakes that struck Hawaii's southeast coast, the great Ka'u earthquake of 1868 (*M*7.9) and the 1975 Kalapana earthquake (*M*7.2), ruptured significant lengths of the fault zone [*Wood*, 1914; *Wyss*, 1988;

Figure 1. (opposite) (a) Shaded slope map of the south flank of Kilauea volcano on the island of Hawaii (white line denotes the shoreline; depth contoured at 1000 m). The 8°–12° slope is blanketed by fragmental basalts, which give way to the east to rougher terrain indicative of submarine erupted lavas. The southwest edge of Kilauea's mobile flank is bounded by an offshore lineament defined by ridges and scarps, including Papa'u seamount (PS) and Nali'ikakani Ridge (NR); box denotes area of detail in Figure 2. The upper flank is marked by two embayments (dark hachures): Halape Bay (HB) shoreline reentrant, between Nali'ikakani Point (NP) and Apua Point (AP), and a central flank embayment above a midslope basin. A broad outer bench extends across the width of the mobile flank and fronts the midslope basin, which is partly filled with volcaniclastic sediment. The steep outer slope of the bench is incised by several arcuate scarps (white hachures) with talus piles and debris flows at their bases. Discrete blocks, hummocky morphology, and relative shallowing of the seafloor, indicated by deflections of the 5000 and 5250 m (dotted) contours, suggest a local avalanche deposit in front of the flank. Seismic reflection lines presented here are indicated by heavy lines with shot point annotations and nearby seismic lines are indicated by lighter lines. Bathymetry is gridded at 100 m from *Smith et al.* [1994]. (b) Map of south flank domains discussed in text. The term "Hilina slump" has commonly been applied to the entire deformed submarine flank of Kilauea, fronted by the outer bench and outlined in bold. We distinguish the active Hilina slump as the coherent portion of the flank showing evidence for downslope displacement, coincident with the western flank shown here by pattern of vertical lines. The central embayment is white and midslope basin is speckled. GPS ground displacement vectors resolved for time interval 1990–1996 [*Owen et al.*, 2000] are superimposed.

Tilling et al., 1976; *Lipman et al.*, 1985]. Trilateration and subsidence measurements following the Kalapana earthquake indicated net downslope movement of the slump block, with up to 8 m seaward displacement and 3.5 m subsidence near Halape Bay [*Lipman et al.*, 1985]. The mean displacement vector for the coseismic slump motion was directed significantly more southward (~S25°–30°E) than time-averaged background displacement trends for the rest of the south flank since 1896 [e.g., *Swanson et al.*, 1976; *Lipman et al.*, 1985; *Denlinger and Okubo*, 1995], suggesting that downslope motion of the Hilina slump is superimposed upon steady flank motion.

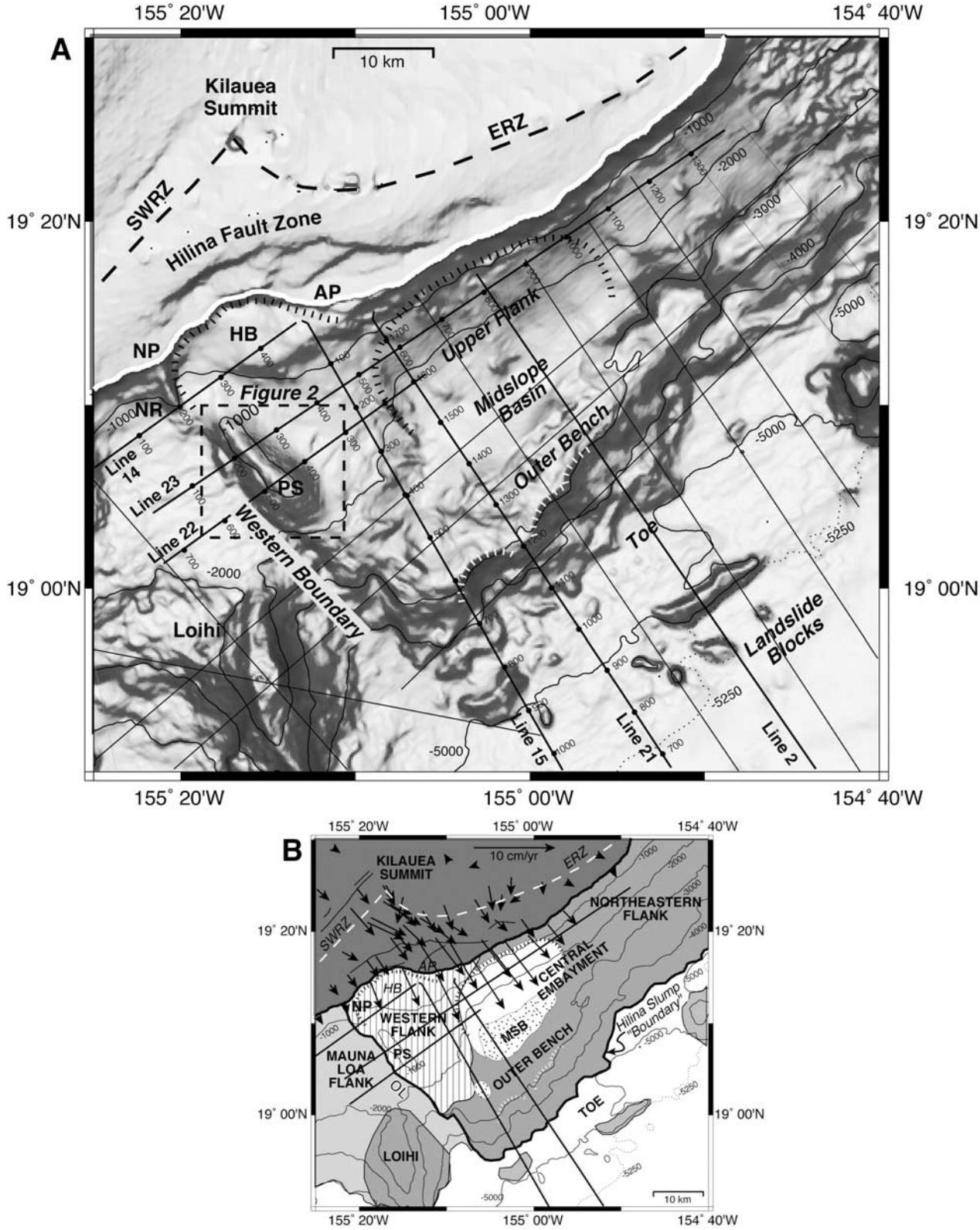

[8] Seaward flank displacements have become more clearly resolved in recent years [e.g., *Owen et al.*, 1995, 2000; *Delaney et al.*, 1993, 1998]. For the time period 1990–1996, uninterrupted by large flank earthquakes, global positioning system (GPS) measurements indicate that the surface of the south flank has crept seaward at rates up to 10 cm/yr [*Owen et al.*, 1995]. Even higher rates of seaward motion, ranging up to 40 cm/yr, were measured prior to 1983 and the onset of the ongoing rift eruptions [*Delaney and Denlinger*, 1999]. Flank motion is in response to gravitational relaxation of the volcanic edifice, assisted by pressurized magma beneath the summit and rift zones [e.g., *Swanson et al.*, 1976; *Dieterich*, 1988; *Iverson*, 1995; *Delaney and Denlinger*, 1999], generally termed volcanic spreading [e.g., *Borgia*, 1994]. Seaward displacement is accommodated by slip along a decollement horizon modeled near the base of the volcano [e.g., *Owen et al.*, 1995, 2000], probably facilitated by sediments on the oceanic plate [e.g., *Nakamura*, 1980; *Iverson*, 1995] or viscous dunite beneath the edifice [*Clague and Denlinger*, 1994].

[9] The geometry and extent of the submarine Hilina slump are poorly known; interpretations have relied largely on offshore morphology and only sparse subsurface data [e.g., *Moore and Chadwick*, 1995; *Smith et al.*, 1999]. Some have assigned the entire south flank of Kilauea to the Hilina slump (e.g., Figure 1b), interpreting the Hilina fault zone to dip quite steeply, intersecting the subedifice decollement, and mobilizing a deep-seated landslide that encompasses the flank [*Lipman et al.*, 1985; *Moore et al.*, 1989, 1994; *Denlinger and Okubo*, 1995]. This interpretation is supported by tomographic evidence for a near-vertical region of low seismic velocities beneath the fault zone [*Okubo et al.*, 1997]. Within this framework, the laterally continuous outer bench (Figure 1) has been interpreted as a downdropped slump block [e.g., *Lipman et al.*, 1985; *Moore et al.*, 1989], or more recently, the result of internal shortening and uplift at the toe of the slump [e.g., *Denlinger and Okubo*, 1995; *Smith et al.*, 1999; *Lipman et al.*, 2002]. Alternatively, the Hilina slump is a shallow feature, possibly confined to the slope sediments upon the upper flanks [e.g., *Moore and Fiske*, 1969; *Swanson et al.*, 1976; *Hill and Zucca*, 1987].

[10] The western edge of the Hilina slump coincides with the southwest boundary of Kilauea's creeping south flank, marked by a prominent set of southeast trending ridges and scarps that extend downslope from Nali'ikakani Point (Figure 1). Relative uplift along the northeast side of this trend reflects right lateral strike-slip motion accommodating seaward displacement of the northeastern block, equated here with the mobile south flank of Kilauea [*Moore and Chadwick*, 1995; *Denlinger and Okubo*, 1995]. The more stable flank to the southwest is influenced primarily by the underlying, less active, Mauna Loa volcano. Papa'u seamount is a prominent high along the western boundary of Kilauea's flank and rises up to 1000 m above the surrounding seafloor (Figure 1). Several interpretations have been proposed for Papa'u: (1) a volcanic construction upon Kilauea's flank [*Emery*, 1955; *Macdonald and Abbott*, 1970; *Smith*, 1996], (2) a large sandy debris lobe derived from the collapse of the upslope shoreline [*Moore and Peck*, 1965; *Moore and Fiske*, 1969; *Fornari et al.*, 1979], or (3) a compressional structure due to convergence between the Hilina slump and Mauna Loa's flank [*Moore and Chadwick*, 1995]. Other features along the boundary, such as the narrow, nearshore ridge referred to as Nali'ikakani Ridge, and the small, asymmetric ridge just west of Papa'u seamount, West Ridge (Figure 1), likely also relate to faulting along the boundary.

[11] The northeastern boundary of the Hilina slump is not apparent from the submarine bathymetry (Figure 1). Downslope of the subaerial edifice, the slopes are draped by a blanket of fragmental basalts and hyaloclastic debris formed by seawater quenching of shoreline crossing lava flows [*Moore et al.*, 1973; *Clague et al.*, 1994; *Moore and Chadwick*, 1995]. This sediment cover thins to the northeast and gives way to the rougher morphology of submarine basalts over the Puna Ridge, without a distinct change in grade.

[12] The south flank is also characterized by several embayments. Halape Bay defines a coastal reentrant below the high cliffs of Pu'u Kapukapu, floored by a shallow shelf (Figure 1). A broad recess marks the central portion of the upper submarine flank, downslope of the ERZ. The embayed flank grades downslope into a broad midslope basin trapped behind the outer bench (Figure 1). Slope angles over the embayed central flank are 11°–12°, measurably steeper than those to the northeast (~9°) and the southwest (~6°–8°).

3. SIMRAD EM300 Bathymetry Over Papa'u Seamount and Adjacent Seafloor

[13] New high-resolution bathymetry, collected using a 30 kHz multibeam SIMRAD EM300 sonar system, hull mounted on the M/V *Ocean Alert* [*MBARI Mapping Team*, 2001], yields unprecedented images of the western boundary of Kilauea and Papa'u seamount. With vertical and horizontal resolution of approximately 2.0 and 0.2% of water depth, respectively, the bathymetric data reveal fine surface details, including shallow slump faults, erosional gullies, and linear terraces that cut the southwestern slopes of Papa'u seamount (Figure 2). Several low-relief, arcuate ridges lie along the seaward base of the seamount. These morphologic features are characteristic of deformation of poorly consolidated slope sediments and unlike volcanic morphologies observed elsewhere around the island (e.g., Loihi seamount; Figure 1). This evidence argues strongly against a constructional volcanic origin for Papa'u.

[14] The new bathymetric data also help to pinpoint the location and attitude of the western boundary fault that accommodates seaward displacement of Kilauea's flank. The trace of the fault lies within the narrow valley separating Papa'u seamount and the smaller West Ridge, and continues upslope along a bathymetric step down to the southwest (Figure 2). On the regional bathymetry, the fault trace follows the east side of Nali'ikakani Ridge (Figure 1). The asymmetric West Ridge just west of Papa'u has a planar eastern slope with the same attitude (11°–13° to the northeast) as Papa'u's northeastern slope (Figure 2). Sharp truncation of this surface along the ridgeline of West Ridge suggests relatively recent exposure. We interpret this surface to be the fault plane of the east dipping boundary fault that dips beneath Papa'u seamount (Figure 2).

[15] Evidence for right-lateral strike-slip displacement along the western boundary fault is provided by apparent

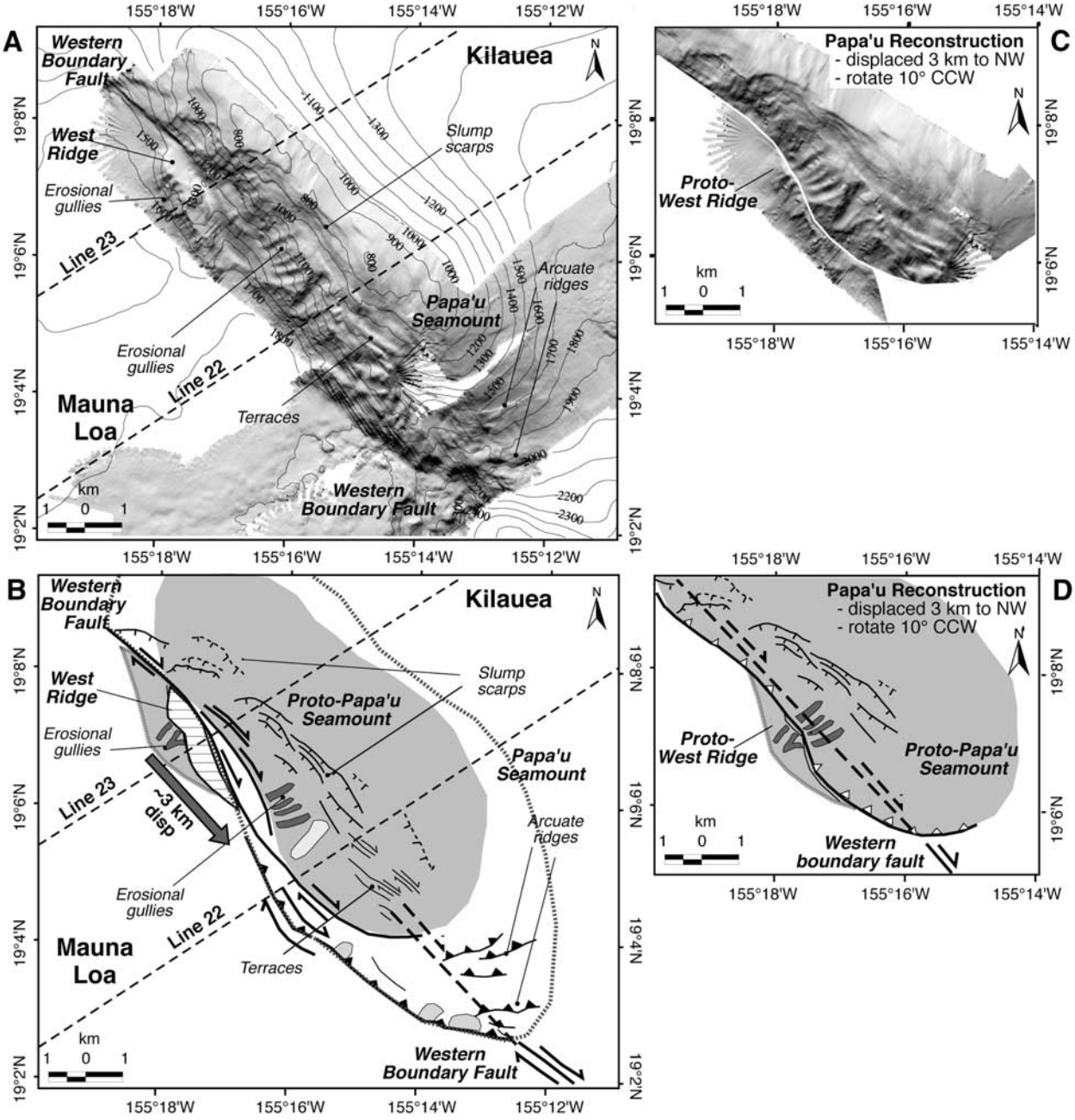

Figure 2. (a) High-resolution SIMRAD EM300 bathymetry data [*Clague et al.*, 1998; *MBARI Mapping Team*, 2001] over Papa‘u seamount (box on Figure 1), gridded at 30 m and illuminated from the northeast. Contours for surrounding area from *Smith et al.* [1994] bathymetry are overlain. Locations of Lines 22 and 23 are shown. (b) Structural interpretation of current configuration of western boundary from SIMRAD data. Boundary fault lies between Papa‘u and West Ridge, and accommodates predominantly strike-slip motion. A distinct set of erosional gullies (dark gray) appears to be offset along the fault. Solid triangles mark upthrown side of active thrust faults. Slump scarps and incipient normal faults are indicated by tick marks on downdropped side. The main Papa‘u ridge is interpreted to have detached from the small western ridge, moving seaward a minimum of 3 km. The planar, northeastern slope of the western ridge (hachured) may represent the surface of the western bounding fault. (c) Reconstruction of Papa‘u seamount, juxtaposing offset erosional gullies and slope of Papa‘u seamount, indicating ~3 km upslope displacement and 10° counterclockwise rotation of eastern block. (d) Interpreted geometry of proto-Papa‘u seamount, prior to downslope displacement. Erosional gullies overprint slump scarps, indicating significant folding predated offset along fault.

offset of deep erosional scours along the nearby slopes. Four parallel gullies crosscut the faulted southwest slope of Papa'u and are abruptly truncated at their downslope edges (Figure 2). A larger gully obliquely crosscuts the set of smaller incisions. The southwest slope of West Ridge also shows similar erosional gullies that are truncated at the ridgeline. These two sets of erosional scours on either side of the western boundary fault can be juxtaposed with a very good fit by displacing Papa'u seamount upslope 3 km, with a 10° counterclockwise rotation; the resulting surface slopes also match quite well (Figure 2). The offset gullies appear to have crosscut preexisting slump faults along Papa'u's southwest flank, indicating relatively recent fault-parallel displacement following early uplift of the seamount. We propose that proto-Papa'u seamount was originally a smaller structure than the present ridge, and grew through continued southeast displacement and oblique slip (Figure 2).

[16] The new SIMRAD data support the interpretation that Papa'u seamount and adjacent seafloor structures result from deformation of Kilauea's submarine flank along the western boundary fault. The preservation of offset morphologic features suggests that fault-parallel displacement along the fault is recent, and most likely, ongoing. From these data alone, it is not clear if the western boundary deformation is due to slumping or seaward displacement of the mobile flank. The seismic reflection data allow us to extend these findings into the deformed submarine flank to determine the subsurface structure of this region.

4. Seismic Reflection Data

[17] We collected 29 MCS reflection lines on board the R/V *Maurice Ewing* over the south flank of the island of Hawaii (Figure 1), forming a three-dimensional network of cross sections intersecting the deep structure of the submarine flank of Kilauea volcano and adjacent seafloor. Several previous papers describe observations across the distal regions of the submarine flank and Hawaiian Moat [*Morgan et al.*, 2000; *Hills et al.*, 2002; *Leslie et al.*, 2002]. Here we focus on several seismic reflection profiles that cross the upper flanks and southwestern margin of Kilauea's mobile flank, to delineate the geometry and evolution of the Hilina slump.

4.1. Data Acquisition and Processing

[18] The seismic reflection data were acquired using a 4 km, 160 channel streamer. The seismic source was a tuned 4336 cubic inches (71 L) air gun array. Each of the lines was processed similarly using Landmark's ProMAX software. The initial parameters and standard processing sequence are summarized in Tables 1a and 1b. We carried out interpretations on stacked and migrated data plotted in two-way travel time (TWTT) and on depth converted sections (Appendix A).

Table 1a. Standard Seismic Data Acquisition Parameters

	Description
Source	15 air guns 4336 cubic inches (71 L)
Receivers	4200 m long streamer 160 channels at 25 m spacing
Shot interval	50 m
Recording	SEG-D format, 2 ms interval

Table 1b. Standard Seismic Data Processing Sequence

	Sequence
1	Resample to 4 ms
2	Edit bad shots and channels
3	Sort to CMP[a] (forty fold, 12.5 m)
4	Band-pass filter (4-8-72-80 Hz)
5	Velocity analysis and dip move out
6	Normal move out correction
7	Forty fold CMP[a] stack (±deconvolution)
8	Low-pass filter for multiple (0-0-35-45 Hz)
9	Migration in F-K[b] domain
10	F-K[b] filter to remove dipping reflections
11	Conversion to depth

[a]Common midpoint.
[b]Frequency wave number.

[19] Seismic imaging through volcano flanks is complicated by a variety of factors [e.g., *de Voogd et al.*, 1999; *Hills et al.*, 2002]. In our area, irregular, often chaotic, volcanic deposits commonly show relatively poor reflector coherence and significantly attenuate the seismic signal. Rough seafloor topography scatters seismic energy and generates out-of-plane reflections and diffractions that are difficult to interpret. The hard seafloor produces strong multiples that can obscure key reflections, particularly in shallow regions. Detailed discussion of various processing techniques used to improve the quality of the seismic data is given by *Hills et al.* [2002] and *Leslie et al.* [2002]. Despite these challenges, the R/V *Maurice Ewing* seismic data provide surprisingly good images of the substructure of Kilauea's submarine flank, which can be interpreted within the context of seafloor morphology, submersible observations, and on-land geology and geodetics.

[20] Due to the shallow seafloor in our study area, multiple suppression was critical to allow us to image subsurface reflections. We employed several techniques to remove strong multiple returns, including prestack and poststack frequency wave number (F-K) filtering, waveform deconvolution, low band-pass filtering to reduce high-frequency multiples, and muting of near-offset multiple returns [e.g., *Hills et al.*, 2002]. We also had good success with radon filtering techniques, wherein multiple returns are modeled and removed in the time intercept, offset domain of common midpoint (CMP) space [*Yilmaz*, 1987]. For our lines, the best multiple reduction was obtained using a combination of techniques, specifically a radon filter with a parabolic 200 ms filter, followed by application of inside mute and low band-pass filter. Radon filtering was applied over residual move outs up to 2000 ms, to deal with the shallow seafloor over much of the area. In regions of particularly high relief, such as Papa'u seamount, no combination of techniques completely removed steeply dipping multiple returns (e.g., Figure 3). In these areas, underlying reflections could be recognized on stacked sections that were selectively filtered to remove high-frequency multiples and steeply dipping reflections and diffractions.

[21] Many of the stronger returns in our seismic data are followed by trains of low-frequency reverberations, which occasionally mask underlying events (e.g., Figure 3). These reverberations can be reduced through deconvolution, but no single technique was appropriate across the entire data set. Prestack deconvolution not only helped to enhance deep

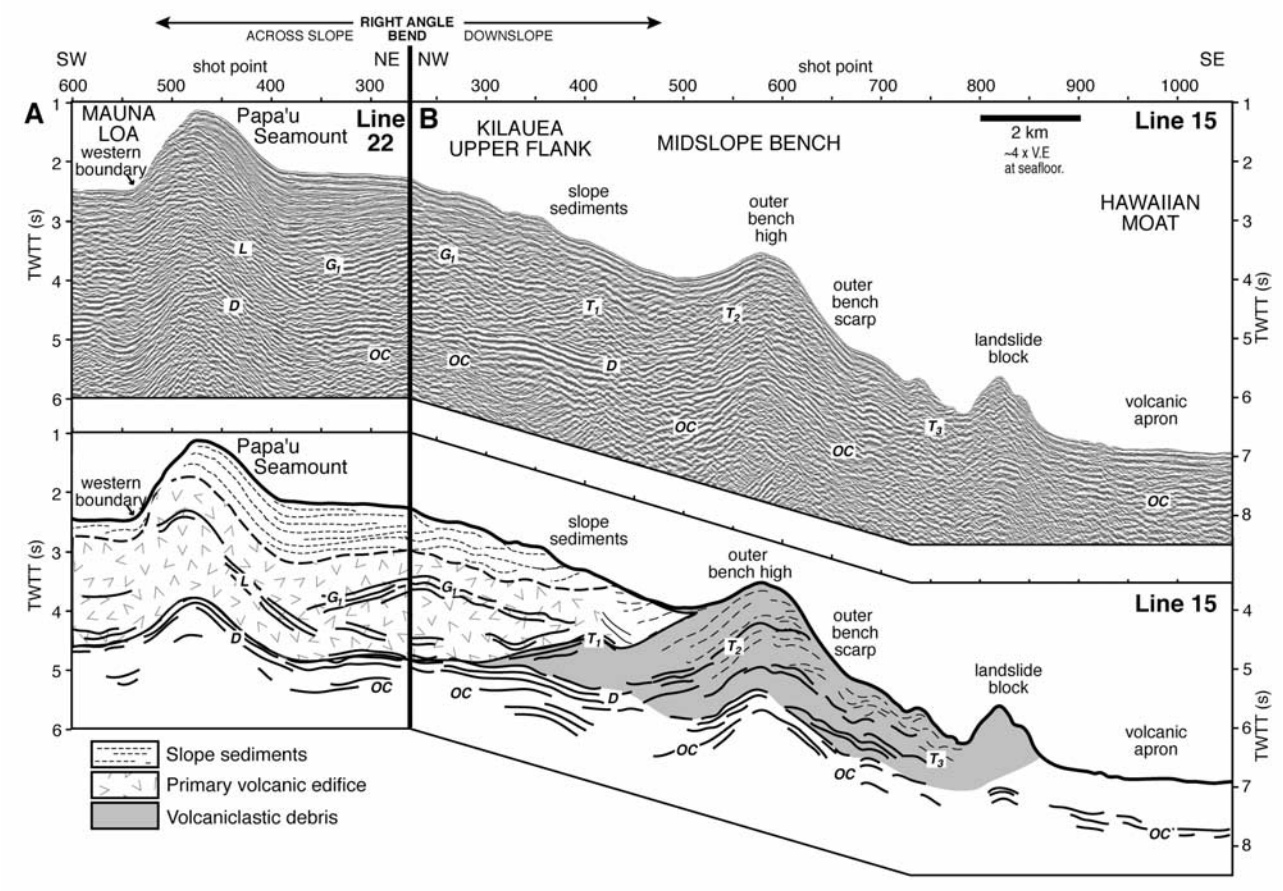

Figure 3. Time sections of intersecting MCS lines crossing the upper flank, and interpretations, showing prominent deep reflections, and seismic domains. (a) Line 22, which crosses the western boundary, Papa'u Seamount, and the upper flank. (b) Line 15, which crosses the upper flank, outer bench, and Hawaiian Moat. Deconvolution has been applied to both lines prior to stacking to enhance the deep reflections; in this display, reverberations from the seafloor reflection obscure shallow bedding reflectors. Strong reflections at 5 and 5.4 s beneath upper flank correspond to the basal decollement (D) beneath the flank and ocean crust (OC), respectively. Characteristics of overlying strong reflections, e.g., D, L, G_1, and T_1, are discussed in the text. The OC reflection is pulled up by high-velocity material beneath the midslope bench at 5.5 s on Figure 3b, but can be followed seaward into the Hawaiian Moat to ~7.2 s. Automatic gain control (AGC) of 500 ms applied.

reflections, but also introduced strong reverberations at the seafloor that obscured important sedimentary features. To gain the most from the data set, we display multiple processed versions of the seismic data below. Poststack deconvolution improved the resolution of deeper reflections, but severely attenuated reflection amplitudes and degraded shallow arrivals; this technique was therefore used only to confirm reflection interpretations, and corresponding profiles are not shown here.

4.2. Results and Interpretation

4.2.1. Top of the Oceanic Plate

[22] We introduce the regional seismic characteristics and common reflections through the compilation of two intersecting MCS lines, Lines 22 and 15 (Figure 3). One of the most prominent sets of reflections identified on the MCS sections occurs between 5 and 6 s TWTT beneath the outer bench and can be followed to ~5 s and less beneath the upper flank and Papa'u seamount. The depth of this reflection below the seafloor, its projection beneath sediments within the Hawaiian Deep (e.g., Figure 3b), and its continuity across the flank [*Hills et al.*, 2002] indicate that this reflection lies near the top of Cretaceous oceanic crust and its sediment cover [*Morgan et al.*, 2000; *Leslie et al.*, 2002]. Based on structural geometries within the outer bench, *Hills et al.* [2002] found the strongest reflection just above and parallel to the oceanic crust to be a basal decollement, D, upon which the mobile south flank of Kilauea slides seaward [e.g., *Nakamura*, 1980; *Denlinger and Okubo*, 1995]. The ocean crust reflection, OC, can be distinguished locally 0.2–0.5 s below D (e.g., Figure 3b; SP 400, 5.2 s). The reverberant character between reflections D and OC may arise from chert beds within the pelagic sediments, as noted within the Hawaiian Moat [*Leslie et al.*, 2002].

[23] The OC and D horizons (Figure 3) are assumed to be nearly planar beneath the submarine flank, dipping 3°–6° toward the island [*Hill and Zucca*, 1987; *Got et al.*, 1994].

On time sections, however, these planar reflections are highly distorted due to velocity pull-up beneath topographic highs such as the outer bench and Papa'u seamount (Figure 3). The apparent distortion of the OC and D reflections on time sections provides a measure of seismic velocity variations within the volcanic flank, allowing us to convert time sections to depth to interpret structural relationships. The method used for depth conversion is described in Appendix A.

4.2.2. Seismic Stratigraphy

[24] The seismic characteristics of the MCS sections across the study region help to resolve three compositional domains (Figure 3): a region of high-frequency, slope-parallel reflections extending up to 1 s below the seafloor, presumed to consist of fragmental subaerially erupted lavas forming a thin blanket of bedded slope sediments; a deeper, less reflective zone above the strong D and OC reflections, characterized by discrete low-frequency and reverberant reflections, defining the primary volcanic edifice composed of submarine erupted pillow basalts; and a frontal domain corresponding to the midslope bench and basin (e.g., Line 15, SP 500–900), composed largely of volcaniclastic debris [e.g., *Morgan et al.*, 2000; *Lipman et al.*, 2002].

[25] Several prominent reflections in addition to D and OC are found across the study area; these are classified and labeled in Figure 3 according to their positions within the flank, geometries, and associations with other reflections. An east dipping reflection, L, rises from the D beneath Papa'u seamount (Line 22, SP 350–500), and is distorted by velocity pull-up beneath the bathymetric high. L is found on all of the western boundary lines and is interpreted to mark the projection of this boundary to depth. A distinct set of middepth reflections, labeled G_1, occurs between 1 and 2 s below the seafloor on both Lines 22 and 15; the internal G_1 reflections do not intersect either seafloor or decollement, but tend to bound unconformable sequences of layered strata, discussed in detail below. Line 15 displays a series of landward dipping reflections that rise from D beneath the lower reaches of the upper flank and midslope bench (SP 400–800); these correspond to frontal thrust faults that have been described previously [*Morgan et al.*, 2000; *Hills et al.*, 2002], and are labeled according to their proximity to the island, i.e., T_1, T_2, and T_3.

4.2.3. Papa'u Seamount and Upper Flank

[26] Line 23 spans much of the upper flank (Figure 1) and reveals contrasting character of the slope sediments along its length (Figure 4). The western portion of the upper flank supports a thick package of coherent, well-bedded, but locally deformed strata, up to 1 s or 1–1.5 km thick. The coherent strata extend nearly 15 km across the flank from the southwestern boundary (SP 200) to a break in slope marking the central flank embayment (SP 500). The interior of Papa'u seamount (SP 200–300) is clearly imaged as a region of thick uplifted strata, defining an asymmetric fold with a long northeastern limb, and bedding reflector terminations against the steeper southwestern face of the ridge (SP 200). A thin wedge of correlative sediments overlies Mauna Loa's slope southwest of Papa'u (SP 1–150) and appears to fold upward into the small West Ridge at the base of the seamount (SP 150–175). The portion of the western flank imaged by the adjacent Line 22 (Figure 5; see also Figure 3a), features a broad syncline developed to the east of the Papa'u fold in the deepest bedded unit (SP 200–400; gray unit). Younger slope sediments onlap to both the east and west, and are folded into the northeast limb of Papa'u (SP 380–450).

[27] Line 22 (Figures 3a and 5) and Line 23 (Figure 4) show similar relationships among the deeper reflections to the east of Papa'u: D lies between 4.3 and 4.6 s; the middepth reflection G_1 occurs between 3.5 and 4 s slightly below the layered slope strata; and the east dipping reflection, L, parallels the northeast limb of Papa'u (e.g., Figure 3a; SP 360, 4.4 s). Reflection L is locally obscured by the shallow seafloor multiple and resulting migration noise beneath Papa'u, but projects toward the southwestern base of the seamount where the trace of the western boundary fault is recognized in the SIMRAD bathymetry (Figure 2).

[28] To the east of the break in slope, well expressed on Line 23, seafloor depth increases across the central bathymetric embayment. This region displays thinned slope sediments in which bedding reflections are difficult to discern (Figure 4, SP 550–750). Locally, small packets of coherent but convoluted sediments occur (e.g., SP 670–730, 2.5–3.2 s). Across the embayed region, a series of discontinuous low-frequency reflections, labeled G_2, underlies the thinned strata (SP 550–750, 3.5–4 s), at a depth similar to that of G_1 to the west. The southwestern edge of the embayment is marked by steps in the seafloor and apparent east directed normal offset of bedding reflections (e.g., SP 470 and 500). To the northeast, a wedge of well-bedded slope sediments has filled a low in the seafloor (SP 800–1000). East dipping bedding reflectors terminate against a southwest dipping boundary (SP 900–950, 2.8–2.2 s), which projects to the seafloor at a small step down to the southwest (SP 1000). Several deeper reflections have been offset to the southwest along this boundary. A package of coherent, slope-parallel bedding reflections, ~0.5 s thick, drapes the slopes northeast of the flank embayment (SP 1000–1200) and grades downward into less reflective but still layered strata.

[29] We interpret these lines to show that along the western slopes of the upper flank, slope strata composing Papa'u seamount have been uplifted and folded along an east dipping fault, L, that defines the western boundary fault. The extensive decollement horizon, D, coincides with that recognized on previous seismic lines, and has accom-

Figure 4. (opposite) Line 23, crossing Papa'u seamount, the western boundary, and the central flank embayment. (a) Uninterpreted, migrated time section shown at ~6.5 vertical exaggeration (V.E.) at the seafloor showing stratigraphic relationships, e.g., coherent strata upon the western flank, dipping beds within Papa'u seamount, thinned and disrupted strata within the central flank embayment. Gray unit correlates on several lines and is discussed in the text. AGC of 200 ms applied. (b) Uninterpreted migrated time section with prestack deconvolution applied to enhance deep reflections, shown at ~4 times V.E. at the seafloor. AGC of 500 ms applied. (c) Interpreted version of Figure 4b. Reflections interpreted as slip planes or faults, e.g., D, L, G_1, and G_2 are indicated by dark bands; the OC is denoted by light bands. Arrows mark sense of offset at the seafloor. See text for discussion.

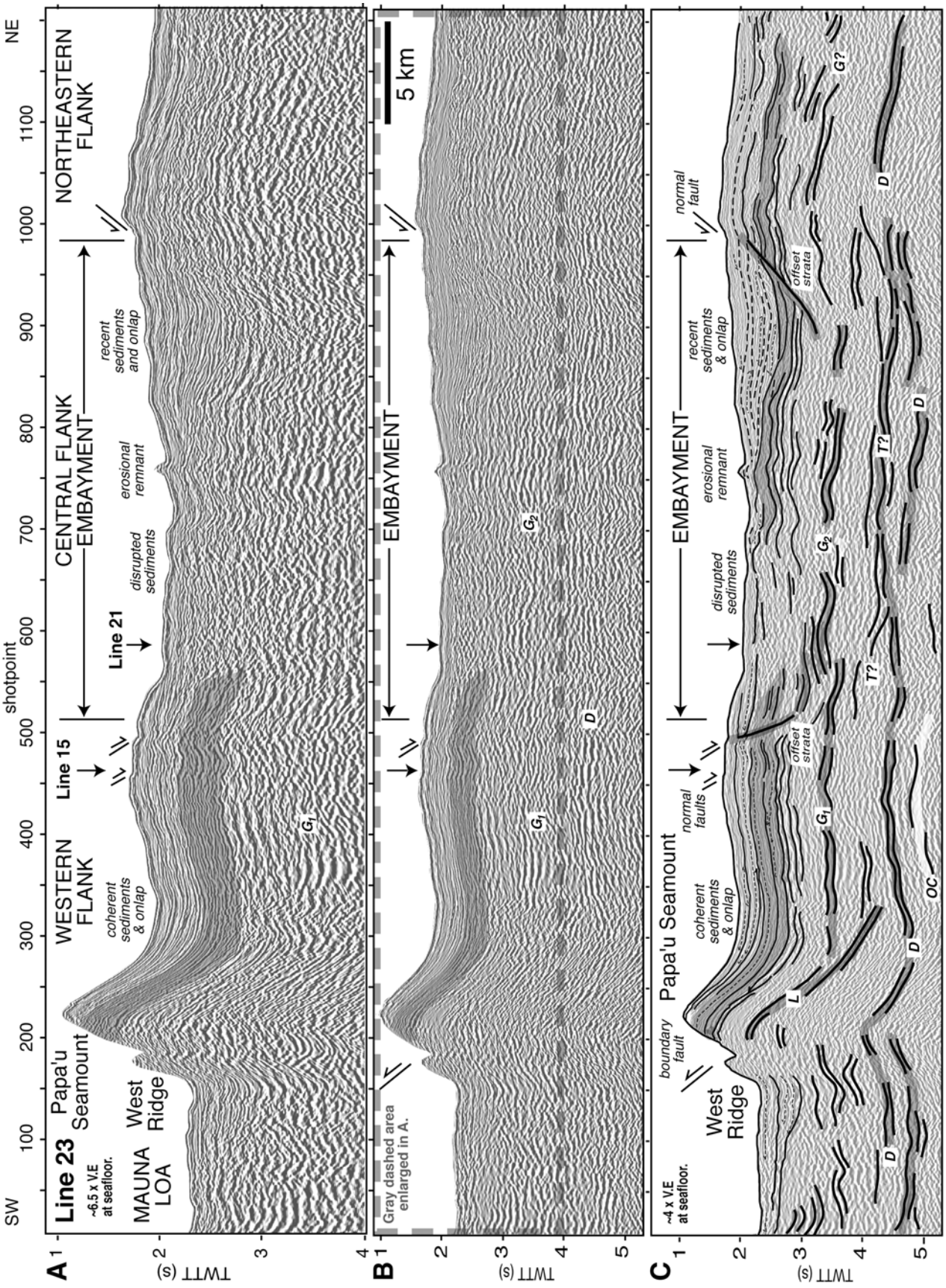
SW
NE
shotpoint
100
200
300
400
500
600
700
800
900
1000
1100
A
B
C
TWTT (s)
Line 23
Papa'u Seamount
West Ridge
MAUNA LOA
~6.5 x V.E at seafloor.
WESTERN FLANK
coherent sediments & onlap
Line 15
CENTRAL FLANK EMBAYMENT
Line 21
disrupted sediments
erosional remnant
recent sediments and onlap
NORTHEASTERN FLANK
G_1
Gray dashed area enlarged in A.
5 km
G_2
D
boundary fault
normal faults
offset strata
T?
L
OC
~4 x V.E at seafloor.
normal fault
G?

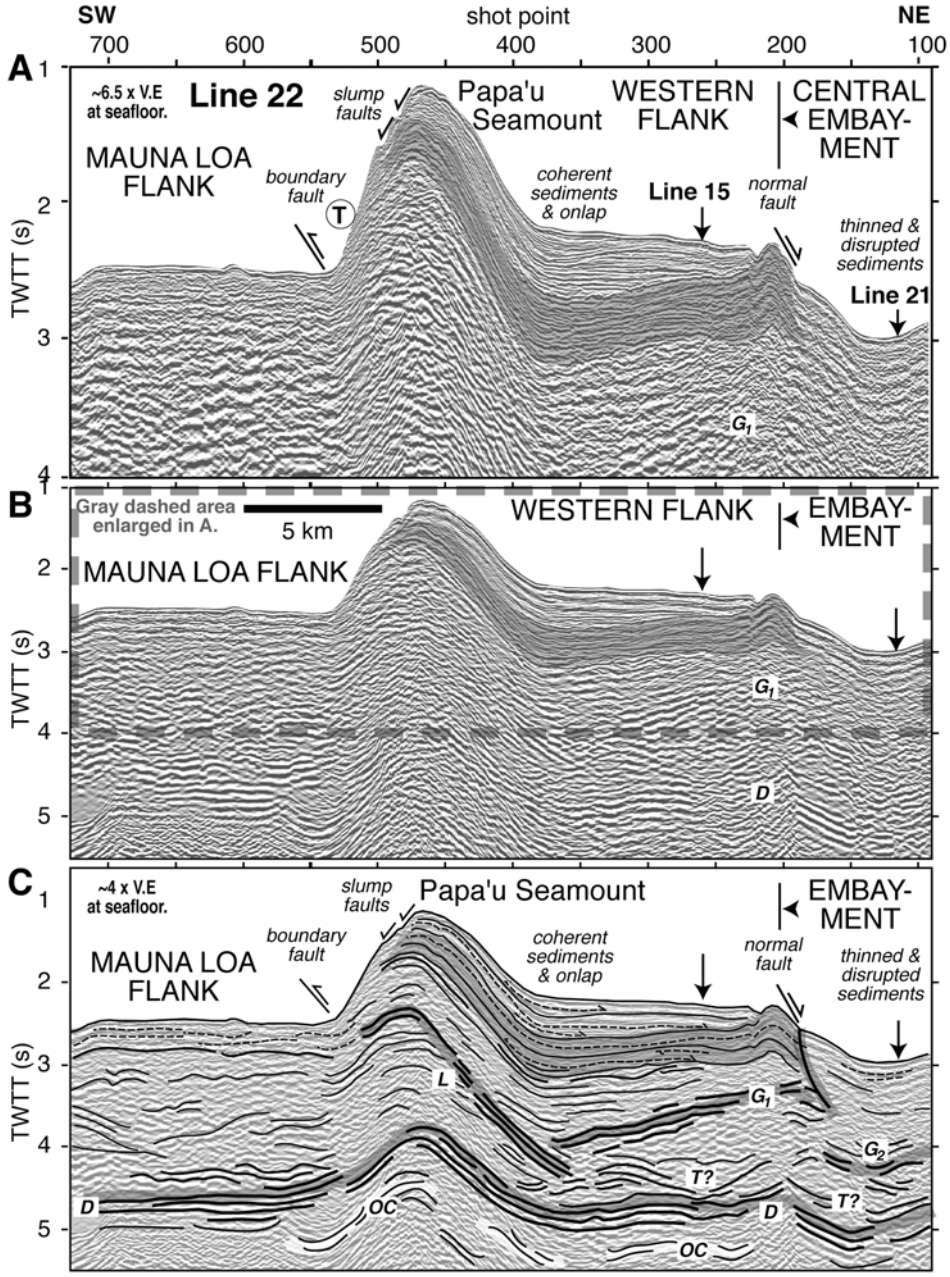

Figure 5. Line 22, crossing Papa‘u seamount, the western boundary, and the west edge of the central flank embayment. (a) Uninterpreted migrated time section showing stratigraphic relationships, such as coherent strata upon the western flank, onlap within the syncline to the east of Papa‘u seamount and dipping beds within Papa‘u. (b) Uninterpreted migrated time section with prestack deconvolution applied to enhance deep reflections. (c) Interpreted version of Figure 5b showing dipping internal G_1, G_2, and L reflections. Symbols and V.E. are as in Figure 4. See text for discussion.

modated largely out of the plane motion [e.g., *Morgan et al.*, 2000]. The two middepth reflections, G_1 and G_2, underlie the deformed slope strata, suggesting that these surfaces have accommodated downslope sliding. Stratal disruption and thinning is greatest to the northeast, within the central embayment, where normal offsets along the boundaries of the embayment suggest a broad region of faulting and slope collapse. Nearly, the entire package of slope sediments has been disrupted within the embayed region; only a thin unit,<0.25 s, appears to postdate slope failure.

4.2.4. Nali’ikakani Ridge and the Shallow Shelf

[30] Closer to shore on Line 14, a slightly different picture of Kilauea’s western boundary is revealed (Figure 6). Nali’ikakani Ridge (SP 160–210) is constructed of west dipping strata, which are buried by slope-parallel sediments to the southwest. The dipping beds are truncated and offset along the east face of Nali’ikakani Ridge, producing a 250 m high scarp (SP 200–210). Small, west dipping normal faults also cut the shallow shelf east of the trough (SP 320–470). Within the fault-bounded trough, a disturbed package of west

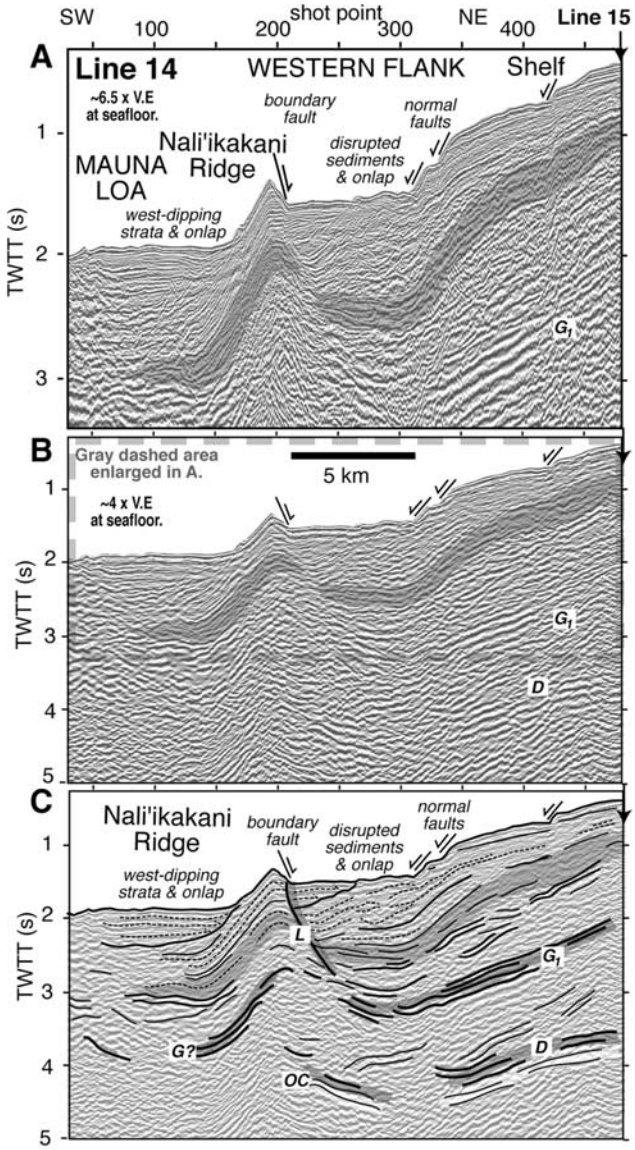

Figure 6. Nearshore Line 14 crossing Nali'ikakani Ridge, the western boundary, and the shallow shelf. (a) Vertically exaggerated, uninterpreted migrated time section showing west dipping strata within the ridge, and east directed offset along the east face of the ridge. Recent, slope-parallel sediments bury a disturbed unit of west dipping strata and normal faults break the shelf. (b) Uninterpreted migrated time section with prestack deconvolution applied to enhance deep reflections. (c) Interpreted version of Figure 6b highlighting dipping G_1 and L reflections. Symbols and V.E. are as in Figure 4. See text for discussion.

dipping strata, probably offset from those in Nali'ikakani Ridge, is buried by younger, slope-parallel sediments (SP 210–310). We are able to correlate the deep-bedded slope unit from Line 22 (gray unit, Figure 6), which also appears to be offset across Nali'ikakani Ridge.

[31] The substructure of Nali'ikakani Ridge (Figure 6) also differs from that of Papa'u seamount. Reflection terminations along the northeast face of Nali'ikakani Ridge and diffuse returns at depth define an east dipping discontinuity, possibly correlated with L, that extends beneath the sediment-filled trough (SP 200–270, 2–3 s). A pronounced west dipping set of reflections beneath the shallow shelf (SP 300–470, 2–3 s) matches the depth and geometry of G_1 reflection downslope. Reflections D and OC occur between 3.5 and 4.5 s depth to the northeast (SP 200–450), but are difficult to trace through the migration noise beneath Nali'ikakani Ridge.

[32] Nali'ikakani Ridge may have a common origin with Papa'u seamount, having formed by folding above an east dipping fault parallel to L, here obscured by migration noise beneath the ridge. The west dipping strata within the ridge, however, were subsequently breached by east directed normal faulting, accompanied by seaward displacement of the eastern block along the glide plane G_1. Reflections L and G_1 link the upslope and downslope structures along the western boundary zone.

4.2.5. Dip Line Across the Western Flank

[33] The two dip lines crossing the upper flank region provide contrasting views into the coherent and disrupted regions of the flank, and clarify the 3D geometry of the deep reflections. Line 15 lies to the southwest of the flank embayment and shows thick slope sediments that are locally faulted, producing small steps in the seafloor (Figure 7a; SP 200–400). Several small detached and rotated blocks 200–500 ms below the seafloor are buried by younger slope-parallel sediments (SP 100–150, 180–230 ms). The deepest bedded unit (Figure 7a, gray unit at 300–700 ms below seafloor) is gently folded and corresponds to the bedded unit defining the syncline east of Papa'u on Line 22 (Figures 3 and 5). A planar reflection, 200–300 ms below the seafloor, cuts across and offsets the folded slope sediments (e.g., Figure 7a; SP 250, 2.7 s), and downslope, the deep bedded unit on the upper flank is exposed at the seafloor (SP 375–475).

[34] Deeper flank reflections imaged on Line 15 (Figures 7b and 7c), correlate well with reflections on the strike-parallel lines discussed above (Figures 4–6, also see Figure 3). The decollement reflection D occurs as a prominent, continuous high-frequency reflection followed by a train of low-frequency reverberations between 2 and 2.5 s below the seafloor (e.g., SP 350, 5 s); the ocean crust reflection OC can be locally distinguished from the reverberations (Figures 7b and 7c; SP 400, 5.8 s). A strong internal reflection about 1 s below the seafloor (Figure 7b; e.g., SP 350, 4 s), correlates with G_1 on the crossing Line 22 (Figure 5b; SP 300, 3.8 s; see also Figure 3). Reflection G_1 underlies the folded and faulted slope sediments and projects toward the seafloor just above the outer bench (Figure 7; SP 450). Several landward dipping reflections rise from D beneath the upper flank (e.g., SP 450, 4.5 s) and outer bench, and are best imaged on depth sections (Figure 7d). Landward dipping reflections within the outer bench, T_1 and T_2, bound packages of internally bedded strata (Figure 7d). Along the outer bench scarp, these internal reflections are truncated (Figure 7d; SP 600–700) and occasional blocks lie outboard of the flank (Figure 1).

[35] The seismic data reveal that the shallow slope strata imaged upon the upper western flank on Line 15 are locally deformed by faulting, folding, and block rotation. The middepth horizon, G_1, is well positioned to serve as an

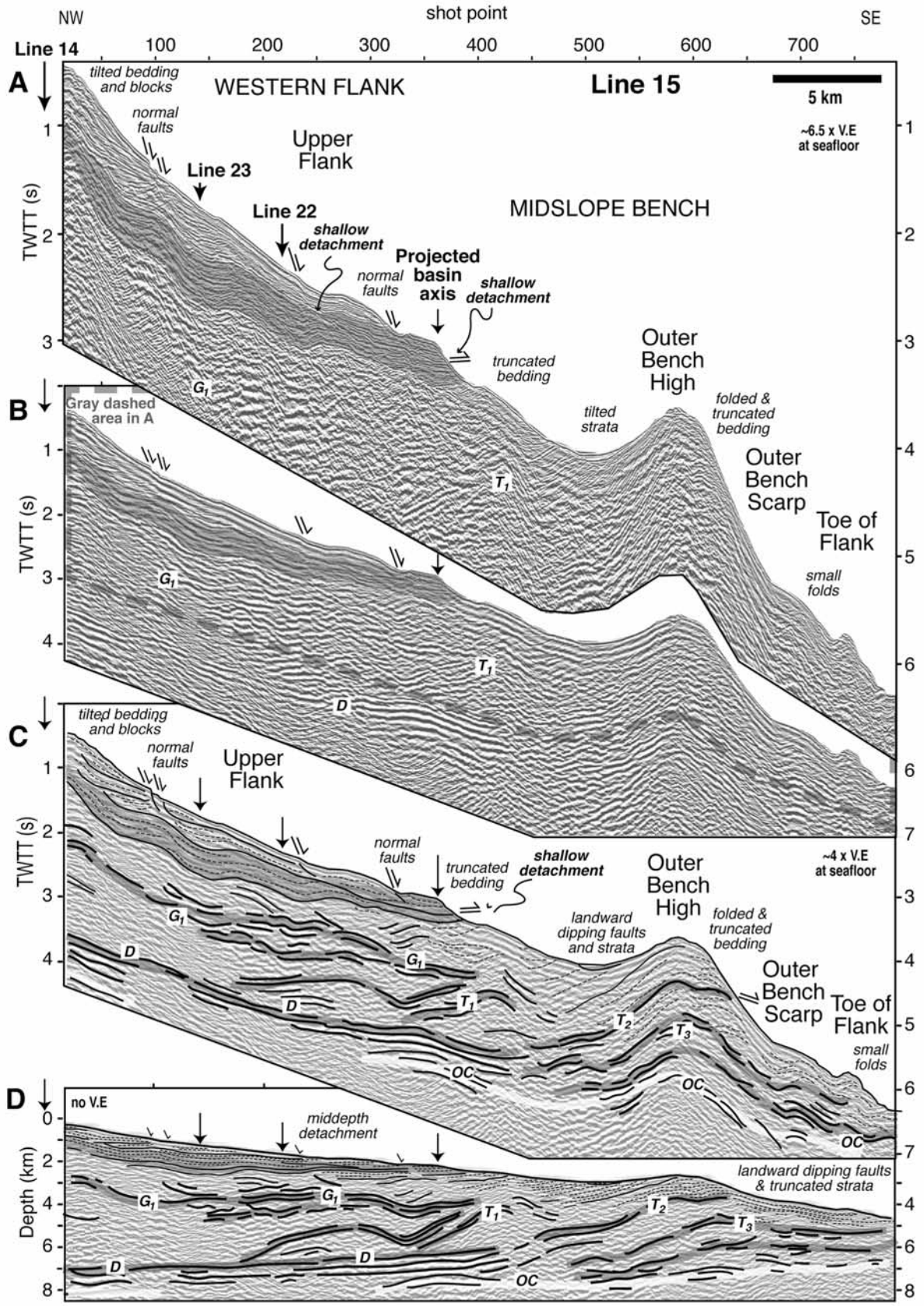
NW
shot point
SE
Line 14
100
200
300
400
500
600
700
A
tilted bedding and blocks
WESTERN FLANK
Line 15
5 km
normal faults
Upper Flank
~6.5 x V.E at seafloor
Line 23
Line 22
MIDSLOPE BENCH
shallow detachment
Projected basin axis
normal faults
shallow detachment
truncated bedding
Outer Bench High
folded & truncated bedding
tilted strata
Outer Bench Scarp
Toe of Flank
small folds
TWTT (s)
B
Gray dashed area in A
C
tilted bedding and blocks
normal faults
Upper Flank
normal faults
truncated bedding
shallow detachment
~4 x V.E at seafloor
Outer Bench High
landward dipping faults and strata
folded & truncated bedding
Outer Bench Scarp
Toe of Flank
small folds
D
no V.E
middepth detachment
landward dipping faults & truncated strata
Depth (km)
G1
T1
T2
T3
D
OC

internal glide plane, lying below the deformed slope sediments and terminating just landward of the midslope bench. Slope units have been faulted and exposed at the seafloor downslope, above the termination of G_1, suggesting slumping of the overlying blocks. The strong, continuous decollement, and landward dipping structures rising from D, record seaward displacement of the south flank, accompanied by thrust faulting at the edge of the upper flank and within the outer bench.

4.2.6. Dip Line Across the Central Flank

[36] Slope strata within the embayed flank region, crossed by Line 21 (Figure 8), are thinner and less coherent than those to the west on Line 15, as suggested from Line 23 (Figure 4). Contorted and tilted, high-frequency reflections define packets of deformed slope sediments (e.g., SP 1460–1530, ~3.8 s and SP 1550–1600, 3.5–4.0 s), which are now buried by well-bedded slope-parallel sediments. The reflective surficial sediments extend unbroken into a broad midslope basin (SP 1375–1550). Line 21 also shows several continuous slope-parallel reflections (SP 1550, 4.5 s-SP 1720, 2.8 s), correlated with G_2 on Line 23. This reflection set underlies the disrupted slope sediments and terminates just behind the midslope basin below several folds marked by convoluted reflections (SP 1450–1550). The basin is filled by well-bedded sediments that onlap the outer bench high (SP 1375–1400) and are now tilted landward at the seaward edge of the basin.

[37] The deep structure of the flank and outer bench crossed by Line 21 resembles that of Line 15, and is clarified on the depth section (Figure 8d). The separate reflections defining D and OC are not as prominent as on Line 15, but can be distinguished beneath the outer bench (e.g., SP 1300, 5.1 and 5.7 s, respectively). As on the neighboring line, landward dipping reflections rise from D beneath the upper flank and bound layered strata within the outer bench. Bedding reflectors are truncated along the upper surface of the outer bench and the steep outer scarp (SP 1100–1200). Several small folds are defined by fine layering near the toe of the flank (SP 1050–1100).

[38] The evidence from Line 21 confirms the interpretation that the embayed region of the submarine flank has been subjected to slope failure and slumping. Small packages of crumpled debris piled up behind the midslope basin and were subsequently buried by young slope sediments and basin fill. The midslope basin formed near the base of the central flank embayment as sediments shed downslope were trapped behind the rising bench. Landward tilting of the youngest basin fill indicates ongoing uplift of the bench.

5. Structural Synthesis

[39] The synthesis of seismic characteristics of south flank strata, reflection geometries and associations, and seafloor morphology, allow us to identify three distinct structural domains that make up Kilauea's submarine flank. Geographically, these are defined as (1) the upper western flank, (2) the embayed central flank, and (3) the midslope basin and outer bench (Figure 1b). Two cutaway perspective views of the south flank summarize the structural characteristics of these domains and their relationships (Figure 9).

5.1. Upper Western Flank

[40] The upper western flank domain is bounded upslope by the shoreline of the Halape Bay reentrant, the western boundary fault, and the west edge of the recessed flank (Figure 1). In this region, the flank is blanketed by a continuous, coherent package of slope sediments up to 1.5 km thick; these strata are locally deformed along normal faults in the upslope region and form a broad fold over Papa'u seamount (Figure 9b; Line 22).

[41] The key subsurface structure along the western boundary is the east dipping lateral fault, L, recognized on all of the slope-parallel lines. Beneath Papa'u, L rises from the decollement D and projects to the seafloor at the southwestern base of the seamount, where offset erosional features pinpoint the trace of the western boundary fault (Figure 2). The east limb of the Papa'u fold lies parallel to L, which therefore has served as a thrust ramp carrying Kilauea slope strata over the more stable flank of Mauna Loa (Figure 9b; Line 22). In contrast to downslope thrusting, the eastern face of Nali'ikakani Ridge is marked by east directed extension, indicating normal displacement along L (Figure 9a; Line 14). The discrepant modes of displacement along the lateral fault L in the two locations can be explained by seaward displacement of a coherent slump block lying to the northeast of the western boundary. Extension along Nali'ikakani Ridge reflects downdropping of the top of the slumped domain, consistent with coseismic subsidence near Halape Bay during the 1975 Kalapana earthquake [*Lipman et al.*, 1985] and the longer record of normal faulting along the on-land Hilina fault system [e.g., *Swanson et al.*, 1976]. Thrusting along Papa'u seamount reflects southwest directed contraction at the toe of the slump.

[42] The middepth reflection G_1 correlates across all the regional seismic lines, and has the proper orientation to define an internal detachment. Reflection G_1 lies about 3–4 km below the seafloor beneath the coherent slope sediments and dips generally south to southwest (Figures 9a and 9b), defining a slump that thickens toward the western boundary. The slump thins to the northeast (Figure 9b; Line 22) and downslope, where the overlying strata are highly faulted and folded (Figure 9a; Line15), possibly due to traction during slip along the shallow detachment. Other deep structures within the upper flank, such as several low-angle reflections noted on Line 15 landward of the outer

Figure 7. (opposite) Line 15, crossing the coherent portion of the western upper flank and outer bench. (a) Vertically exaggerated, uninterpreted migrated time section showing coherent strata on upper flank, locally folded and faulted, along normal faults that offset the seafloor. Outer bench is composed of layered, landward dipping strata. (b) Uninterpreted migrated time section with prestack deconvolution applied to enhance deep reflections. (c) Interpreted version of Figure 7b, showing dipping G_1 reflections ~1–1.5 s below seafloor, approaching seafloor above outer bench. Symbols and V.E. are as in Figure 4. (d) Depth section, converted as described in Appendix A, showing landward dipping reflections rising from D within outer bench. No vertical exaggeration. See text for discussion.

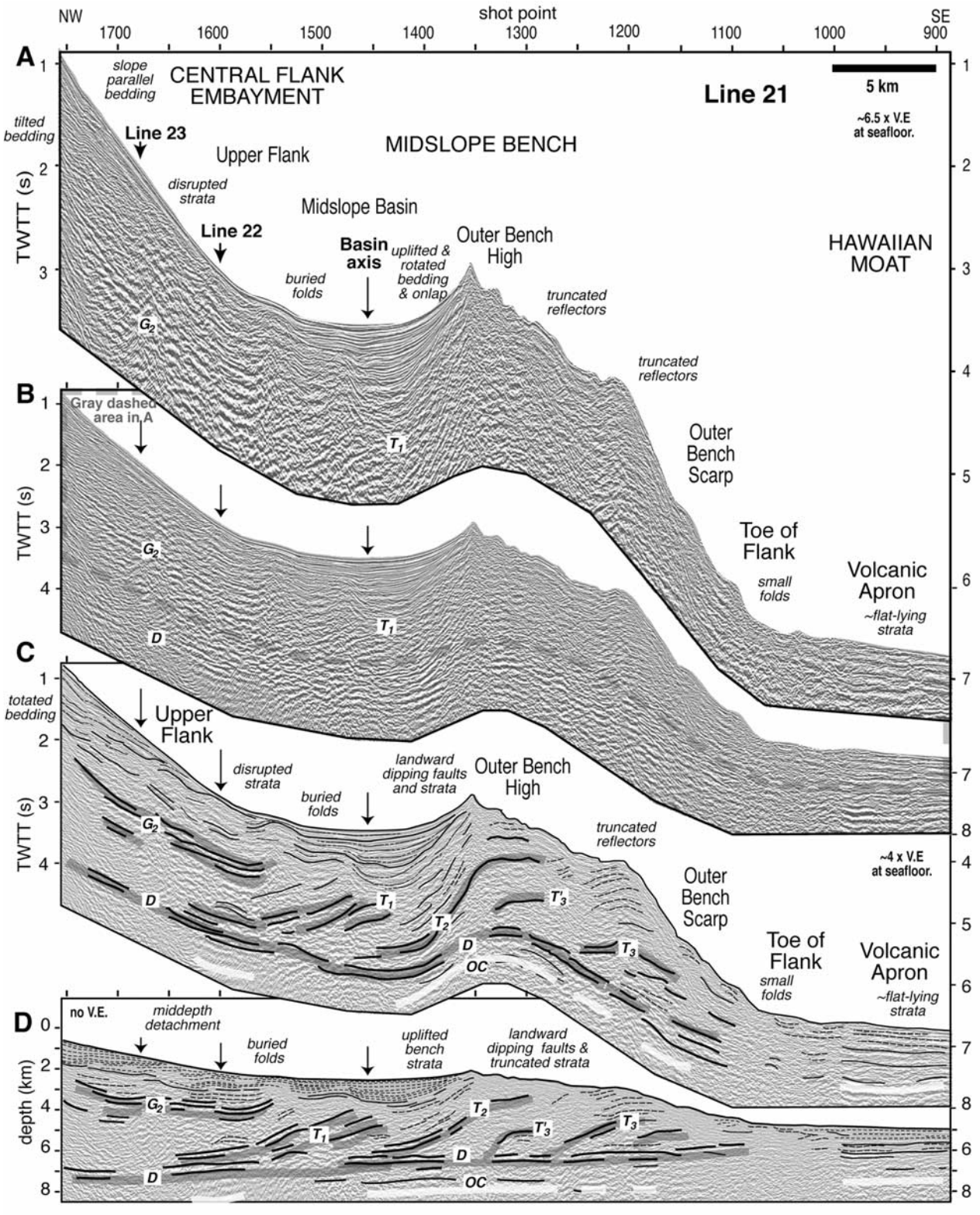

Figure 8. Line 21, crossing the central flank embayment, midslope basin, and outer bench. Vertically exaggerated, uninterpreted migrated time section showing thinned disrupted strata on upper flank, overlain by slope-parallel sediments. Midslope basin is filled by well-bedded sediments, which onlap outer bench and are tilted landward. Outer bench is composed of layered, landward dipping strata. (b) Uninterpreted migrated time section, with prestack deconvolution applied to enhance deep reflections. (c) Interpreted version of Figure 8b, showing dipping $G_2 \sim 1$ s below seafloor, underlying contorted stratal reflections now buried by basin fill. Symbols and V.E. are as in Figure 4. (d) Depth section, showing landward dipping reflections rising from D within outer bench. No vertical exaggeration. See text for discussion.

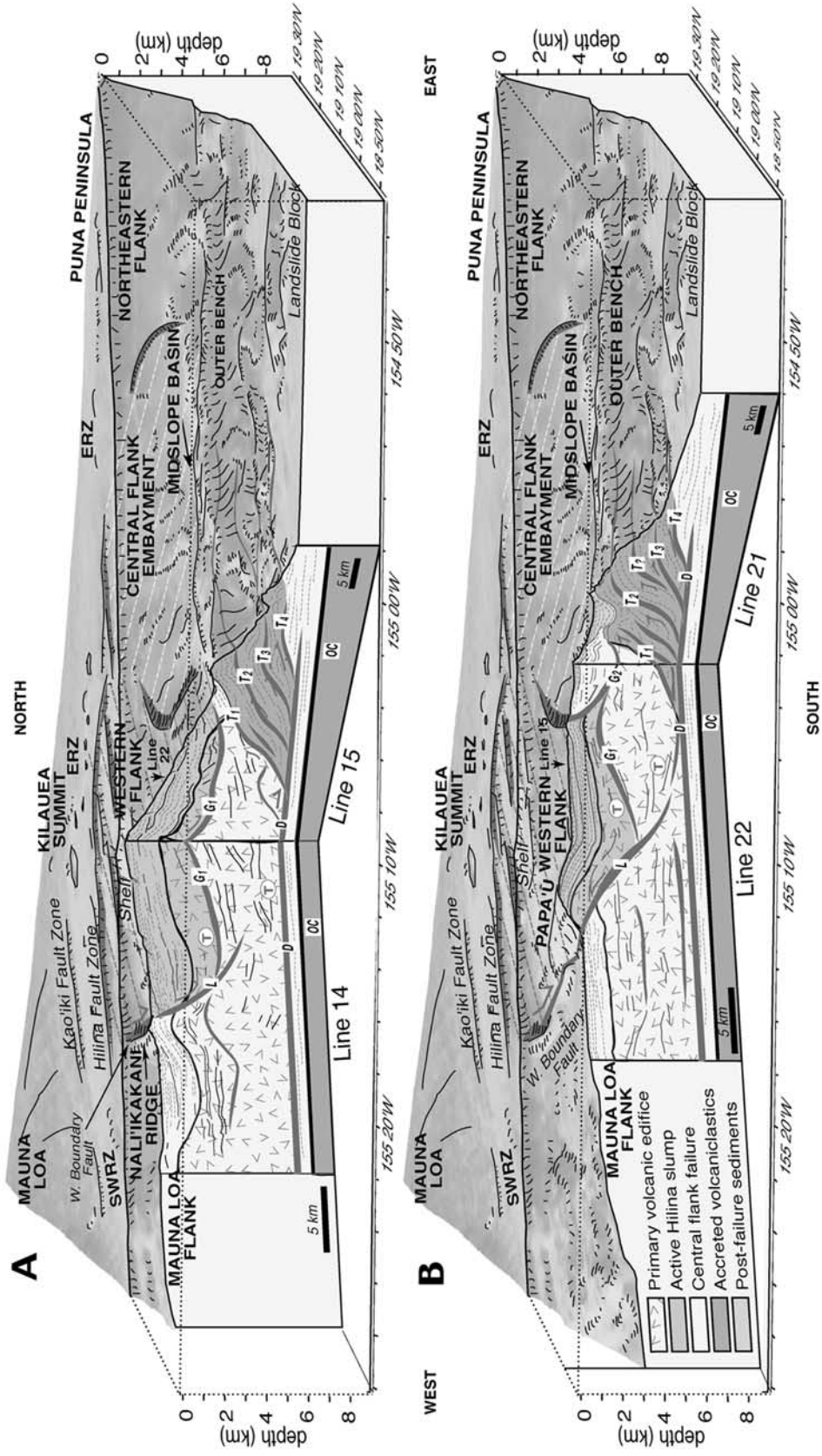

Figure 9. Cutaway views through Kilauea's south flank showing subsurface structures compiled from the seismic data. (a) Lines 14 and 15 reveal the structure of the western flank, detachment G_1, and the Hilina slump. Extension along Nali'ikakani Ridge, and folding and faulting of the shallow sediments on Line 15 result from downslope movement of the Hilina slump. Deeper structures are primarily landward dipping, accommodating thrusting and accretion of volcaniclastic strata within the outer bench. (b) Lines 22 and 21 show uplift and westward thrusting of Papa'u due to oblique convergence of the Hilina slump upon the western boundary fault. The transition to the region of central flank failure is marked an arcuate scarp at the seafloor, and listric G_2 detachment at depth. Imbricate thrust sheets within the outer bench front the central flank embayment, ponding sediments within the midslope basin. See color version of this figure at back of this issue.

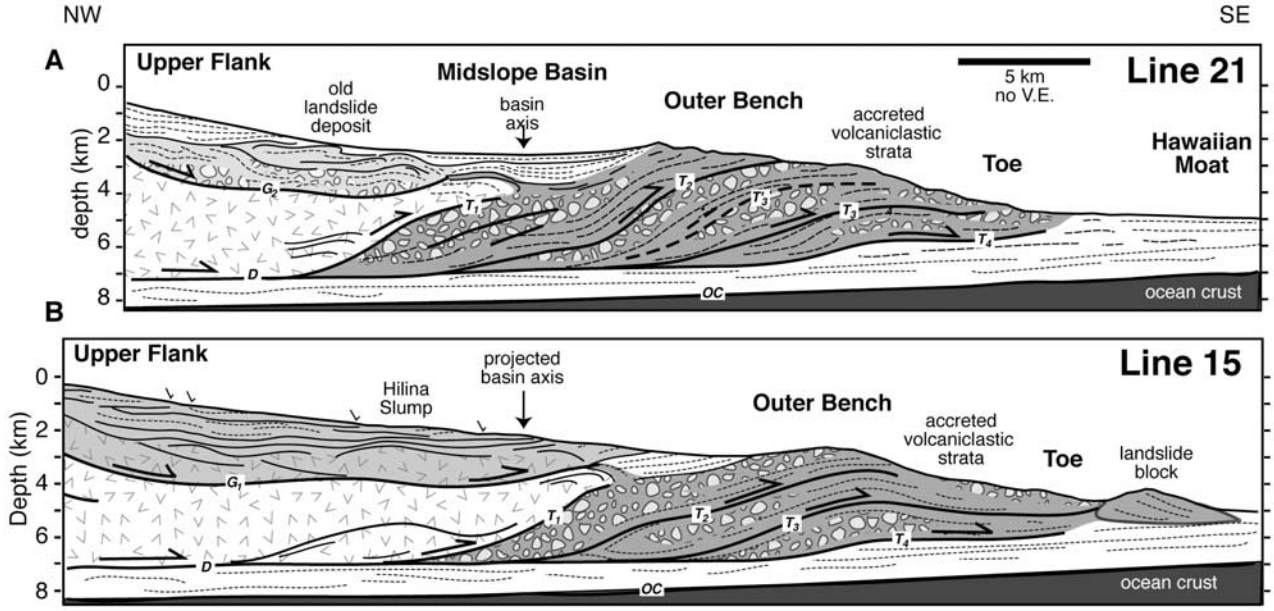

Figure 10. Interpreted depth sections for dip lines: (a) Line 21 and (b) Line 15; symbols are as in Figure 3. The two transects, aligned along the axis of the midslope basin show contrasting structure. Disrupted strata underlie bedding parallel slope and basin sediments on Line 21, whereas Line 15 shows the more coherent Hilina slump. The primary volcanic edifice extends farthest seaward on Line 15 and appears to be truncated beneath the midslope basin along Line 21, where the imbricated stack of accreted volcaniclastic debris is thickest. The uppermost portion of the outer bench has been eroded or detached along Line 21, contributing landslide blocks to the Hawaiian Moat.

bench (Figure 9a; Line 15), appear to relate to deep-seated thrusting at the toe of the flank [e.g., *Morgan et al.*, 2000].

5.2. Central Flank

[43] The seismic characteristics of Kilauea's embayed central flank domain contrast with those of the west. Little coherent bedding is observed, sediment cover is thinned, and the broad midslope basin lies near the base of the upper flank (Figures 1 and 8). Discrete packages of convoluted strata denote significant internal disruption (Figures 8 and 10a), in contrast to the more coherent upper flank strata along the western flank (Figures 7 and 10b). Normal offset faults mark the southwest and northeast edges of the embayment (Figures 4 and 9b). The central flank embayment outlines a large sector of the upper flank that experienced complete detachment and catastrophic collapse sometime in the past. The shallowest sediments, showing continuous, nearly slope-parallel, bedding reflections, have filled in the bathymetric low, burying the disturbed strata and smoothing the steepened slopes (e.g., Figure 8).

[44] The principal detachment surface for the failed central flank is interpreted to be the reflection set G_2 (Figure 9b; intersection of Lines 21 and 22), which lies $\sim$1.5–2 km below the seafloor and dies out in the seaward direction beneath buried, convoluted strata at the landward edge of the midslope basin (Figure 8, SP 1450–1550). The present depth below sea level of G_2 nearly matches that of the G_1 detachment over the western flank, cutting into the primary volcanic edifice below the slope sediments (Figure 10). Collapse of the central flank apparently involved both shallow slope sediments and deeper primary pillow basalts. Both the southwestern and northeastern edges of the central flank embayment show listric geometries and the arcuate form of lateral breakaway faults that may connect to G_2 (Figures 1 and 9). The upslope breakaway fault is not obvious on Line 21, but may now be buried by present-day shoreline deposits. The linkage between the submarine detachment and on-land fault scarps is not observed on our data.

5.3. Midslope Basin and Outer Bench Domain

[45] The outer bench is constructed of a stack of imbricated thrust sheets that have formed in front of Kilauea's mobile flank (Figures 9 and 10). Consistent with interpretations from adjacent lines [*Morgan et al.*, 2000; *Hills et al.*, 2002], the mobile volcanic flank has overthrust and offscraped volcaniclastic strata accumulated within the volcanic apron outboard of the edifice. This construction resembles the anticlinal ridge produced by volcanic spreading, envisioned by *Borgia and Treves* [1992]. The two bench crossing reflection lines, Lines 15 (Figure 10b) and 21 (Figure 10a) reveal seaward verging thrust faults rising from a gently dipping, subedifice decollement D. In our study area, D lies about 1 km above the top of oceanic crust and probably rides along the top of buried pelagic and clastic sediments [e.g., *Nakamura*, 1980; *Denlinger and Okubo*, 1995; *Morgan et al.*, 2000; *Leslie et al.*, 2002]. The thrust faults that built the outer bench (e.g., T_1, T_2, etc.) are laterally continuous and can be correlated between Lines 15 and 21 (Figures 9 and 10), and along strike to adjacent lines examined previously [e.g., *Hills et al.*, 2002]. The layered appearance of the fault-bounded thrust packages suggests

that the thrust sheets consist largely of volcaniclastic breccias and sandstones, which have been found in abundance across the outer bench scarp along Kilauea's south flank [e.g., *Lipman et al.*, 2002; *Sisson et al.*, 2002]. Surface erosion and block detachment have incised the outer bench, shedding landslide blocks that are now found within the Hawaiian Moat (Figure 1).

[46] Despite the similar structure of the outer bench on both Lines 21 and 15 (Figures 9a and 9b), the transition from bench to upper flank is markedly different. Line 21 crosses the midslope basin dammed by the outer bench (Figure 10a). Folding, onlap, and landward dips of sediments within the basin (Figure 8; SP 1370–1430) indicate that bench growth has continued as the basin filled [*Hills et al.*, 2002]. The bench is narrower on Line 15 and supports only a small basin (SP 450–550). The broad basin to the northeast is missing; in its place is found a structural high that corresponds to the toe of the slump that breaks the upper flank (projected basin axis, Figure 10b). The primary volcanic edifice is interpreted to extend at least 2 km farther seaward on Line 15 than on Line 21 (Figure 10) reflecting the flank embayment behind the basin on the latter transect.

6. Discussion

[47] The data presented above reveal a complicated subsurface structure for Kilauea's submarine south flank, resulting from multiple, interacting geologic processes: slumping and slope collapse, erosion and deposition, magmatic intrusion, and volcanic spreading. For the first time, we are able to constrain the extent of submarine slumping and slope failure on the active slope of the volcano and assess the interplay among the different processes acting on the submarine flank.

6.1. Submarine Manifestation of the Hilina Slump

[48] The new seismic reflection and bathymetry data over Kilauea's south flank delineate the offshore boundaries of the Hilina slump and clarify the origin of Papa'u seamount and adjacent morphological features. Our data demonstrate that Papa'u defines a broad fold composed of coherent, layered slope strata, uplifted by southwest vergent thrusting along the western boundary of Kilauea's mobile south flank (Figures 4 and 5). Neither the sandy debris lobe model, arising from collapse and downslope flow of an unstable nearshore lava delta [*Fornari et al.*, 1979; *Moore and Chadwick*, 1995], nor the constructional volcanic interpretation [*Emery*, 1955; *Macdonald and Abbott*, 1970; *Smith*, 1996] are borne out by our data. Seismic reflections within the deeper flank reveal an east dipping boundary fault L upon which Papa'u is built and a middepth detachment G_1 that accommodated downslope movement of the Hilina slump block (Figure 9). Net uplift of Papa'u occurred concurrently with nearshore extension and subsidence along Nali'ikakani Ridge, and normal faulting along the on-land Hilina fault zone, consistent with slump block kinematics.

[49] The structure of Nali'ikakani Ridge is puzzling given the slump model posed above. The boundary ridge is cut by an east directed fault, reflecting subsidence and seaward displacement across the lateral boundary of the slump (Figure 9a). However, the ridge is composed of west dipping strata suggesting prior convergence. The shallow sediments may have been folded during initial stages of flank displacement, concurrent with initial uplift of Papa'u seamount in the downslope regions. This is compatible with uplift and folding of Papa'u prior to formation of the erosional gullies and offset by fault-parallel slip. Convergence between Kilauea and Mauna Loa may have resulted from generally south directed gravitational stresses along this portion of the flank, directed radially away from Kilauea's summit. Rupture of the shallow flank and western boundary fault enabled downslope slumping, accompanied by continuing convergence, matching present-day ground motions [e.g., *Owen et al.*, 2000]. Alternatively, the west dipping strata in Nali'ikakani Ridge represent nearshore fragmental basalt deposits comparable to those accumulating below the lava entry to the northeast (Figure 1). The present-day shoreline now lies some 5 km north of the Line 14 crossing of the ridge; however, colinearity of the seaward edge of the shallow shelf in Halape Bay with the shoreline to the northeast (Figure 1) suggests that the shelf is a submerged portion of the subaerial edifice, and the ancient shoreline may once have extended to Nali'ikakani Ridge, since subsided below sea level.

[50] Papa'u fold apparently grew over a long period of concurrent slope sedimentation. Onlap relationships among the bedded units composing the eastern limb of Papa'u fold and the adjacent trough show that continuous deposition was punctuated by intermittent slump displacement (Figure 5; SP 200–400). Uplift of Papa'u seamount began after deposition of the deepest bedded unit (gray in Figures 4 and 5), which shows relatively uniform thickness across the flank. New geochemical data reveal that this package contains fragmental basalts with Mauna Loa geochemistry, which may predate Kilauea [*Kimura et al.*, 2002]. Onset of uplift along the western boundary trapped pillow basalts and debris derived from Kilauea along the eastern slopes. As Papa'u grew, it incorporated the new strata into its expanding eastern limb, the adjacent trough subsided, and the overlying deposits onlapped the edges of the trough. Uplift of the ridge has continued recently, as even the shallowest slope sediments have been tilted along the eastern flank of the fold (Figure 5; Line 22).

6.2. Geometry and Vergence of the Hilina Slump

[51] The folded strata within Papa'u seamount (Figure 9) and offset erosional markers along Kilauea's western boundary (Figure 2) allow us to estimate the magnitude of displacement and transport direction for the Hilina slump. About 1–1.5 km of fault normal displacement produced the folding of the deepest slope package within Papa'u (Figure 11a). Combined with 3 km of fault-parallel displacement evident from the SIMRAD bathymetry (Figure 2), the net displacement along the fault is slightly more than 3 km along a S $\sim$ 25°E trajectory, oblique to the western boundary.

[52] Our calculated vergence direction for Papa'u seamount closely matches onshore displacement directions determined for the Hilina slump block, but differs from background ground motions for the sliding south flank (Figure 1). Coseismic displacement vectors for the region seaward of the Hilina fault zone during the 1975 Kalapana earthquake yielded a similar vergence direction of S25°–30°E [*Lipman et al.*, 1985]; discrete fault offsets along the Hilina fault system from the Kalapana earthquake, as well

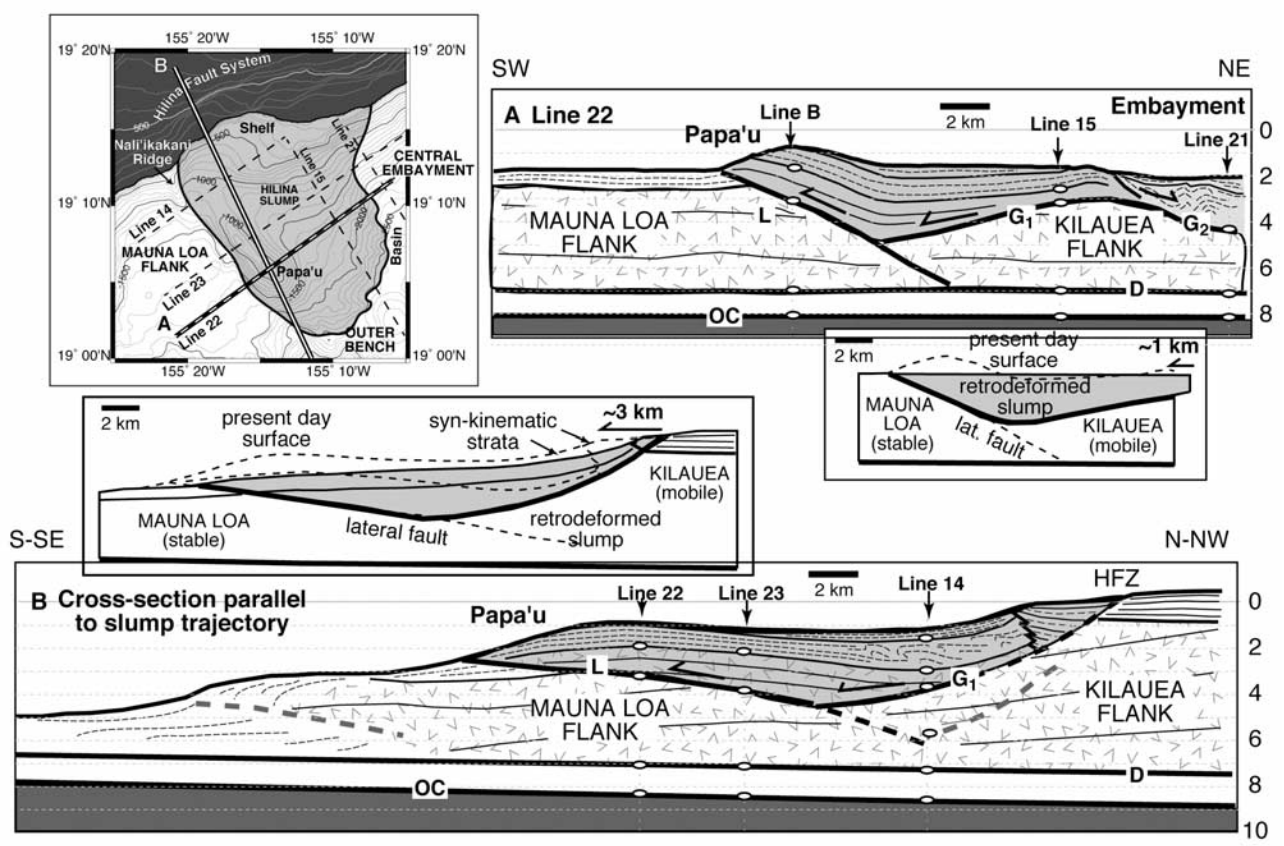

Figure 11. Two structural cross sections across the upper western flank, oriented (a) perpendicular to the western boundary fault (e.g., Line 22) and (b) parallel to the transport direction for the Hilina slump; symbols are as in Figure 3. Ellipses mark depth constraints of reflectors from seismic sections. Insets show reconstructed configurations that can be compared with deformed configuration (dashed). Papa'u records ~1 km fault normal displacement. The slump has experienced about 3 km of downslope displacement, based on offset erosional markers from the high-resolution bathymetry (e.g., Figure 2). The Hilina fault zone is correlated with G_1 in this section, yielding a dip of ~20°–25°. See text for discussion.

as prehistoric events, also indicate a general south-southeast trend [*Cannon and Bürgmann*, 2001; *Cannon et al.*, 2001]. By comparison, cumulative displacement vectors for the creeping south flank measured since 1896 are directed generally southeast [e.g., *Swanson et al.*, 1976; *Lipman et al.*, 1985; *Delaney et al.*, 1998] approximately normal to the central ERZ and the strike of the offshore outer bench [*Hills et al.*, 2002]. Finally, despite little evidence for discrete movement of the Hilina slump since 1975, postseismic GPS measurements across the creeping south flank show a gradual southward deflection of displacement direction, concurrent with a decrease in magnitude, in the vicinity of the Hilina block (Figure 1b): mean flank displacements trend ~S45°E below the central ERZ, about S30°E at Apua Point at the northeast edge of Halape Bay, and more southerly, S15°E at Nali'ikakani Point [e.g., *Owen et al.*, 2000]. This divergence, modest in scale, may result from intermittent aseismic slip along the Hilina detachment, as recently captured following a major rainfall event on the south flank [*Cervelli et al.*, 2002].

[53] Similar vergence directions estimated for both offshore and onshore structures support our interpretation that Papa'u seamount is the submarine manifestation of the Hilina slump, headed along the on-land Hilina fault zone. A balanced cross section constructed parallel to the calculated transport direction (Figure 11b) shows feasible subsurface fault geometries for the slump block, constrained by seismic reflection data presented here. The detachment G_1 is interpreted to be the offshore extension of the Hilina fault zone; the listric geometry of the fault yields an on-land dip of ~20°, shallowing to ~5° at a depth of 3–4 km in the offshore region before merging with the eastern boundary fault (Figure 11b). This shallow, listric fault configuration coincides with other recent models for the Hilina fault, based on coseismic fault slip vectors [*Cannon and Bürgmann*, 2001], ground motions [*Cannon et al.*, 2001; *Cervelli et al.*, 2002], and tsunami data [*Ma et al.*, 1999], as well as paleomagnetic constraints for net rotations of Hilina fault blocks [*Riley et al.*, 1999]. The slump block is composed primarily of slope sediments, as originally hypothesized by *Swanson et al.* [1976]. The underlying detachment may take advantage of a distinct mechanical discontinuity near the base of the sediments. More steeply dipping faults, for example, greater than

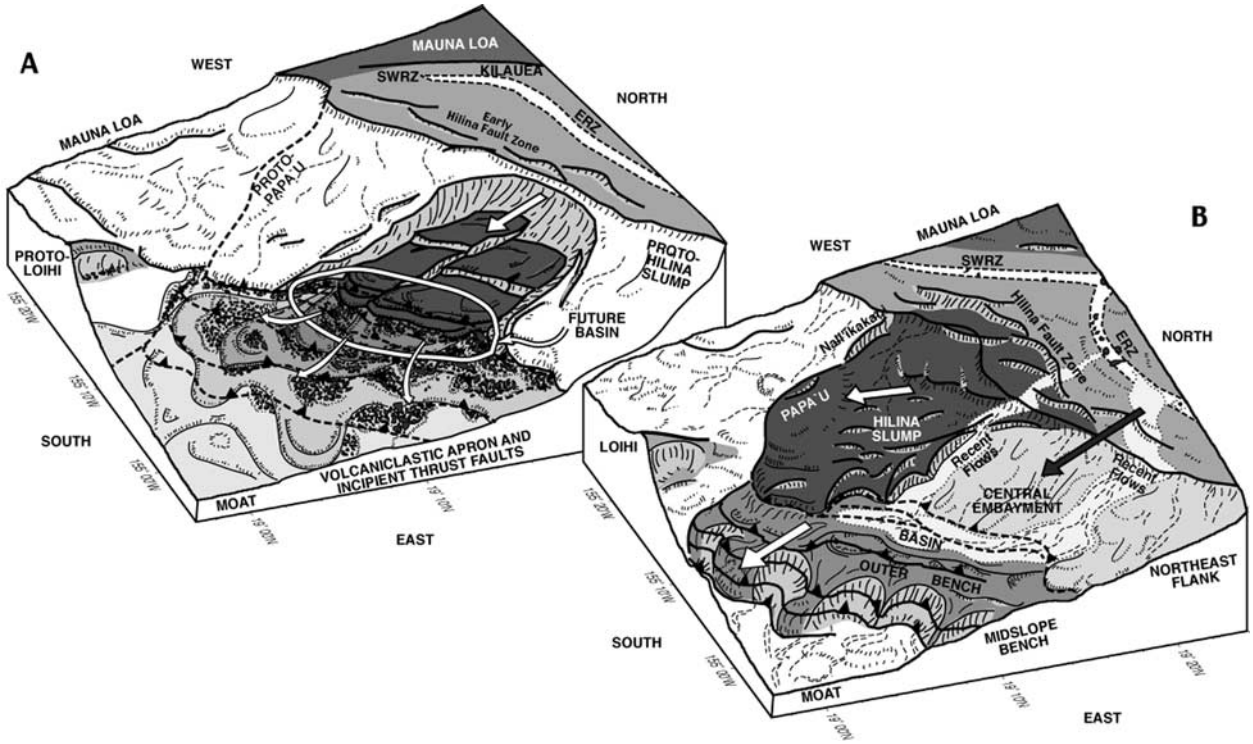

Figure 12. Schematic model for slope collapse and slumping along Kilauea's mobile south flank. (a) The central portion of the large proto-Hilina slump detaches catastrophically, depositing chaotic debris out in the Hawaiian Moat. (b) Collapse of the central sector leads to a change in vergence of the slump, which impinges upon the western boundary fault, uplifting Papa'u seamount. The landslide debris is offscraped by seaward sliding of the south flank, accommodating extension and southward migration of the central ERZ. Young slope sediments fill in the embayment where the collapse occurred and collect in the midslope basin dammed behind the outer bench. The midslope basin marks the position of the recessed toe of the collapsed flank. Recent sediments derived from subaerial lava flows entering the ocean (white) progressively infill the recessed flank and basin, burying the record of past slope failures.

$\sim 60^\circ$ interpreted by others [*Lipman et al.*, 1985; *Moore et al.*, 1989; *Okubo et al.*, 1997] would not be imaged by our offshore reflection data and cannot be assessed here.

6.3. Collapse of the Central Flank and Growth of the Outer Bench

[54] Our MCS data across the upper flank of Kilauea demonstrate that the central portion of the south flank of Kilauea collapsed catastrophically in the recent past. The detachment cut through nearly the entire bedded section of slope sediments, including units that record onset of slip and uplift along the western boundary on Line 23 (Figure 4). Only the youngest strata, which bury the deformed units and spill into the midslope basin and onto the outer bench on Line 21, are relatively undisturbed (Figures 8 and 10). This implies that downslope motion of the slump and convergence along the western boundary predated collapse. The south flank was apparently broken by a much larger proto-Hilina slump of which the central portion broke away.

[55] Detachment of the central block cut through the shallow slope sediments and into the primary volcanic edifice, and distributed a mixture of reworked slope units and underlying volcanic lithologies into the Hawaiian Moat, where they spread out to form a broad volcaniclastic apron (Figure 12a). The hummocky region outboard of the present outer bench (Figure 1) has been interpreted as a remnant of the debris deposit [*Moore et al.*, 1989; *Smith et al.*, 1999], and thick accumulations of chaotic debris are recognized across the frontal moat [*Leslie et al.*, 2002]. However, the laterally continuous outer bench now fronts the collapsed flank effectively damming further dispersal of slope debris. Recent submersible dives along the outer slopes of the bench observed a rich variety of volcaniclastic lithologies from coarse breccias containing a range of subaerial and submarine basalt clasts to well-sorted, subaerially derived hyaloclastic sandstones and conglomerates [*Lipman et al.*, 2002]. A surprising abundance of clasts have alkalic compositions, suggesting that ancestral Kilauea was the source of the rocks [e.g., *Lipman et al.*, 2002; *Sisson et al.*, 2002]. These are interspersed with sands derived from Mauna Loa [*Lipman et al.*, 2002]. The outer bench is now the repository of landslide debris derived from the detachment and breakup of the upper flank, which cut through a thin veneer of young Kilauea overlying the submarine edifice of Mauna Loa volcano (Figure 12a).

[56] The midslope basin outlines the flank embayment behind the outer bench, which can now be understood as the ghost of the underlying landslide scar. The basin was preserved because the adjoining, intact flanks drove thrust faulting outboard of the scar (Figure 12b); only small folds

and thrusts developed within the depression and were subsequently buried by young basin fill, as shown on Line 21 (Figure 8; SP 1450–1550). Intermittently, slumps and debris flows probably detached from the oversteepened upper flank depositing thin packages of chaotic debris within the basin, particularly downslope of the present lava entry [e.g., *Hills et al.*, 2002]. Small ridges exposed at the seafloor (e.g., Figure 4; SP 775) may be remnants of such local erosive events.

[57] The exact cause of the central flank collapse is not known, but we can speculate about possible triggers. Flank seismicity, for example, of the magnitude of the great 1868 Ka'u ($M \sim 8.0$) or the 1975 Kalapana earthquakes (M7.2) would certainly shake the submarine flanks, dislodging precarious slope deposits, but such seismicity accompanies flank sliding and must be ongoing, at least for an extensive period of volcanic evolution. Catastrophic flank collapse of the scale observed here, and documented around the islands, is thought to occur relatively late in the evolution of the volcano [e.g., *Moore et al.*, 1989], and may coincide with unusually energetic volcanic eruptions, perhaps explosive in nature [*Clague and Dixon*, 2000; *McMurtry et al.*, 1999]. Kilauea volcano has experienced at least two extraordinary phreatomagmatic eruptions within the last 50,000 years, both associated with collapse of the summit caldera, and responsible for massive ash deposits dated at 49 and 23–29 ka [*Clague et al.*, 1995]. Such events are certain to break the static equilibrium of the edifice, enabling catastrophic sector collapse.

[58] The breakup of the proto-Hilina slump and collapse of the central flank would have significantly changed the configuration and stress state of the south flank, inducing irreversible changes in the behavior of the volcano [e.g., *Morgan and Clague*, 2003]. Without an anchor to the east, the remnant Hilina slump to the west may have experienced a shift in vergence toward the south-southeast, converging upon the western boundary of the flank. Removal of material from the central flank would have relieved confining stresses acting on the central ERZ, enabling dike intrusion, rift zone extension, and southward migration to form the distinctive bend in the upper ERZ (Figure 1) [*Swanson et al.*, 1976; *Delaney et al.*, 1998]. A concurrent decrease in normal stress acting upon the base of the volcano could also weaken the underlying decollement enabling rapid seaward displacement of the south flank, overthrusting the distal volcaniclastic debris. Discrete thrust sheets were offscraped and accreted to the toe of the sliding flank to form the frontal bench (Figure 12b) [*Morgan et al.*, 2000]. As indicated by uplift and rotation of young strata at the seaward edge of the midslope basin, the bench continues to grow and is the submarine manifestation of on-land seaward creep documented geodetically [e.g., *Swanson et al.*, 1976; *Owen et al.*, 1995, 2000; *Delaney et al.*, 1998].

[59] The remarkable evidence that the bench is a recent construction, postdating a flank failure that disrupted all but the youngest slope units upon the upper flank, implies rapid seaward sliding of the south flank. Although the timing of flank collapse is unknown, we speculate that it may have been triggered by explosive eruptions within 25–50 ka [*Clague et al.*, 1995]. Reconstructions of bench deformation record a minimum of 15 km of displacement [e.g., *Denlinger and Okubo*, 1995; *Lipman et al.*, 2002] and possibly up to 24 km or more [*Morgan et al.*, 2000]. This amount of shortening implies time-averaged displacement rates of 30–60 cm/yr, much higher than present rates measured on land [*Owen et al.*, 1995]. Such high rates are far from unreasonable for the distal flank, which is driven by displacement of the deep volcanic edifice; elastic dislocation modeling of present-day surface displacement rates of ~10 cm/yr implies slip rates along the basal decollement on the order of 15–25 cm/yr [e.g., *Delaney et al.*, 1993; *Owen et al.*, 1995, 2000]. Furthermore, much higher rates of flank migration have been measured in the recent past, e.g., up to 40 cm/yr of surface motion prior to 1983, apparently modulated by internal magma pressures and surface eruptions [*Delaney and Denlinger*, 1999].

6.4. Implications

[60] The Hilina slump, a remnant of the larger proto-Hilina slump, is now restricted to the western portion of Kilauea's mobile south flank. It is still active, as evidenced by recent coseismic displacements [e.g., *Lipman et al.*, 1985] and aseismic slip triggered by rainfall events [*Cervelli et al.*, 2002]. The evidence for previous catastrophic collapse along the central region of Kilauea's south flank cautions us about future detachment of the extant slump block. However, our results suggest that the remnant Hilina slump may be comparatively stable due to its oblique convergence upon the western boundary of the mobile flank and therefore subject only to small intermittent displacements as recorded in the slope strata. Over time, slump activity may lessen even further as downslope motion is increasingly buttressed by the growing outer bench. If this is the case, dire predictions of the future breakaway of the Hilina slump [e.g., *Ward*, 2002] may be overstated, although there are many external factors that may play a role in flank deformation in this active volcanic setting.

[61] The evidence for rapid bench growth along Kilauea's south flank, possibly triggered by precursory slope collapse, suggests that landslides can set off a chain of events that govern volcanic behavior and growth for a long period after, and from which it may never recover. At Kilauea volcano, the picture seems simple enough; collapse of the central flank relieves confining stresses acting on both the ERZ and the basal detachment, enabling south flank sliding. Initially, rapid rates of displacement decay with time, until eventually, the broken flank is regenerated by intrusion, eruption, and slope deposition. Flank sliding ceases until a new cycle begins. A surprising twist in this model, however, is the construction of a large frontal bench at the base of the sliding flank from volcaniclastic debris derived from previous slope failures. As the bench grows it resists flank sliding and buttresses new slumps forming upon the upper flanks. In order to overcome the added resistance, each trigger event must be bigger than the last, and only the largest volcanoes are likely to experience more than one or two such events before they become inactive.

[62] Finally, our observations suggest that the active processes we recognize on Kilauea volcano today are the consequence of changes in south flank configuration and stress state resulting from slope collapse, which we propose occurred relatively recently in the evolution of Kilauea. Therefore we are presently capturing a transient stage in Kilauea's growth that may be decaying, setting the stage for

a new phase, possibly of greater stability. The sequence that we recognize at Kilauea likely has been repeated on many older Hawaiian volcanoes, in particular, Mauna Loa, leaving telltale flank structures and landslide deposits [e.g., *Lipman et al.*, 1988; *Moore et al.*, 1989; *Lipman*, 1995; *Morgan and Clague*, 2003]. However, this pattern may not be representative of the long-term behavior of Hawaiian volcanoes. With this recognition, we can better interpret past events around the islands and throughout the world, and anticipate the consequences of repeated slope collapse along active volcanic islands.

7. Conclusions

[63] New MCS reflection data and high-resolution bathymetry over the southeast submarine slopes of the island of Hawaii demonstrate a history of past catastrophic landsliding and present-day stable slumping along Kilauea's mobile south flank. A continuous blanket of slope sediments up to 1.5 km thick has been uplifted and folded to form the prominent Papa'u seamount along the western boundary of the active flank. Upslope, sediments have undergone extension and subsidence consistent with recent coseismic ground motions of the nearby shoreline. In combination, these structures define a coherent slump that is creeping downslope, probably linked to the on-land Hilina fault zone. Seismic reflection and high-resolution SIMRAD bathymetric data constrain an east dipping fault along the western boundary which accommodates largely right-lateral slump displacement and a detachment plane ~3–4 km below the seafloor allowing downslope motion. Total slump displacement is estimated at slightly more than 3 km in the south-southeast direction, matching coseismic and continuous ground displacement vectors for the Hilina slump block on land, and in contrast with the southeast vergence of the rest of the creeping south flank.

[64] To the northeast, a broad, fault-bounded flank embayment contains thinned and disrupted slope sediments, indicating catastrophic slope failure of the central flank in the recent past. Debris shed from the collapsed flank must have dispersed into the Hawaiian Moat in front of Kilauea, forming an extensive volcanic apron. Seaward sliding of Kilauea's south flank subsequently offscraped these deposits to build the frontal bench, recording up to 24 km of displacement. A broad basin formed above the base of the embayed flank and filled with fragmental debris shed from upslope. Uplift and rotation of the basin fill indicate recent, and possibly continuing, bench growth.

[65] The sequence of deformational events along the south flank of Kilauea suggests a dynamic interplay among slope failure, flank regrowth, and volcanic spreading. Large-scale flank collapse may have triggered seaward sliding of the flank, causing sudden, irreversible changes in the state of stress acting on the rift zone and underlying decollement plane. Present-day flank motions and deformation may represent a transient phase in Kilauea's history, and displacement may cease once the flank regenerates through volcanic growth. The large Hilina slump cuts the surface of the mobile south flank, and has shown recent activity. Catastrophic detachment of this landslide, however, is increasingly unlikely due to buttressing effects of the western boundary fault and the rising midslope bench.

Appendix A: Depth Conversion of MCS Data

[66] Geophysical constraints gained from refraction [e.g., *Hill and Zucca*, 1987], flexure [*Thurber*, 1987], and seismicity [*Got et al.*, 1994] studies indicate that the top of the ocean crust dips 3°–6° landward beneath the south flank of Kilauea and lies at a depth of about 8–9 km beneath Kilauea's summit. We developed velocity models for the volcanic flank using published velocity ranges [*Hill and Zucca*, 1987] in order to return the OC reflection to this dipping planar geometry.

[67] For our purposes, we iteratively construct three velocity layers above the oceanic crust, which marks the base of our region of interest. These correspond to (1) water, with constant velocity of 1500 m/s, (2) bedded sediments with seafloor velocities of ~2200 m/s that increase linearly with depth, and (3) primary volcanic strata, with velocities of 3700 m/s near the top, increasing to about ~5500–6000 m/s at the base, consistent with deep oceanic basalts [e.g., *Salisbury et al.*, 1996]. We have assumed a constant velocity of 6000 m/s for the oceanic plate. The true velocity structure of the submarine flank may differ from our idealized three-layer model, resulting in reflector mislocations up to 200–300 m, however, our depth conversions yield reliable relative positions and geometries of reflections for purposes of structural interpretation.

[68] **Acknowledgments.** We are especially grateful to the helpful and professional shipboard and technical crew of the R/V *Maurice Ewing*, who ensured the success of the Kilauea seismic cruise and the high quality of the MCS data. Denise Hills, Stephen Leslie, and Jackie Caplan-Auerbach assisted with seismic acquisition and processing. Thoughtful reviews by Roland Bürgmann and Daniel Fornari were invaluable in preparing the final manuscript. Beatrice de Voogd and several anonymous reviewers provided helpful critiques of earlier drafts of this paper. Stimulating conversations with many other colleagues, among them Don Swanson, Jim Moore, and Peter Lipman, helped to clarify our geologic thinking. We acknowledge support of this project by Landmark Graphics Corporation via the Landmark University Grant Program. This work was funded by National Science Foundation grant OCE-9711715.

References

Borgia, A., Dynamic basis of volcanic spreading, *J. Geophys. Res.*, *99*, 17,791–17,804, 1994.

Borgia, A., and B. Treves, Volcanic plates overriding the oceanic crust: Structure and dynamics of Hawaiian volcanoes, in *Ophiolites and Their Modern Oceanic Analogues*, edited by L. M. Parson, B. J. Murton, and P. Browning, *Geol. Soc. Spec. Publ.*, *60*, 277–299, 1992.

Cannon, E. C., and R. Bürgmann, Prehistoric fault offsets of the Hilina fault system, south flank of Kilauea volcano, Hawaii, *J. Geophys. Res.*, *106*, 4207–4219, 2001.

Cannon, E. C., R. Bürgmann, and S. E. Owen, Shallow normal faulting and block rotation associated with the 1975 Kalapana earthquake, Kilauea volcano, Hawaii, *Bull. Seismol. Soc. Am.*, *91*, 1553–1562, 2001.

Cervelli, P., P. Segall, K. Johnson, M. Lisowski, and A. Miklius, Sudden aseismic fault slip on the south flank of Kilauea volcano, *Nature*, *415*, 1014–1018, 2002.

Clague, D. A., and R. P. Denlinger, Role of olivine cumulates in destabilizing the flanks of Hawaiian volcanoes, *Bull. Volcanol.*, *56*, 425–434, 1994.

Clague, D. A., and J. E. Dixon, Extrinsic controls on the evolution of Hawaiian ocean island volcanoes, *Geochem. Geophys. Geosyst.*, *1*, Paper number 1999GC000023, 2000.

Clague, D. A., K. A. Hon, J. L. Anderson, W. W. Chadwick Jr., and C. G. Fox, Bathymetry of Puna Ridge, Kilauea volcano, Hawaii, *U.S. Geol. Surv. Misc. Field Stud. Map*, *MF-2237*, 1994.

Clague, D. A., M. H. Beeson, R. P. Denlinger, and L. G. Mastin, Ancient ash deposits and calderas at Kilauea volcano (abstract), *Eos Trans. AGU*, *76*(46), Fall Meet. Suppl., F666, 1995.

Clague, D. A., J. R. Reynolds, N. Maher, G. Hatcher, W. Danforth, and J. V. Gardner, High-resolution SIMRAD EM300 multibeam surveys near the Hawaiian Islands: Canyons, reefs, and landslides (abstract), *Eos Trans. AGU*, *79*(45), Fall Meet. Suppl., F826, 1998.

Day, S. J., S. I. N. Heleno da Silva, and J. F. B. D. Fonseca, A past giant lateral collapse and present-day flank instability of Fogo, Cape Verde Islands, *J. Volcanol. Geotherm. Res.*, *94*, 191–218, 1999.

Delaney, P. T., and R. P. Denlinger, Stabilization of volcanic flanks by dike intrusion, *Bull. Volcanol.*, *61*, 356–362, 1999.

Delaney, P. T., A. Miklius, T. Arnadottir, A. T. Okamura, and M. K. Sako, Motion of Kilauea volcano during sustained eruption from the Puu O'o and Kupai'anaha vents, 1983–1991, *J. Geophys. Res.*, *98*, 17,801–17,820, 1993.

Delaney, P. T., R. P. Denlinger, M. Lisowski, A. Miklius, P. G. Okubo, A. T. Okamura, and M. K. Sako, Volcanic spreading at Kilauea, 1976–1996, *J. Geophys. Res.*, *103*, 18,003–18,023, 1998.

Denlinger, R. P., and P. Okubo, Structure of the mobile south flank of Kilauea volcano, Hawaii, *J. Geophys. Res.*, *100*, 24,499–24,507, 1995.

de Voogd, B., S. Pou Palome, A. Hirn, P. Charvis, J. Gallart, D. Rousset, J. Danobeitia, and H. Perroud, Vertical movements and material transport during hotspot activity: Seismic reflection profiling offshore La Reunion, *J. Geophys. Res.*, *104*, 2855–2874, 1999.

Dieterich, J. H., Growth and persistence of Hawaiian volcanic rift zones, *J. Geophys. Res.*, *93*, 4258–4270, 1988.

Duffield, W. A., L. Stieltjes, and J. Varet, Huge landslide blocks in the growth of Piton de la Fournaise, La Reunion, and Kilauea volcano, Hawaii, *J. Volcanol. Geotherm. Res.*, *12*, 147–160, 1982.

Emery, K. O., Submarine topography south of Hawaii, *Pac. Sci.*, *9*, 286–291, 1955.

Fornari, D. J., J. G. Moore, and L. Calk, A large submarine sand rubble flow on Kilauea volcano, Hawaii, *J. Volcanol. Geotherm. Res.*, *5*, 239–256, 1979.

Got, J.-L., J. Frechet, and F. W. Klein, Deep fault plane geometry inferred from multiplet relative relocation beneath the south flank of Kilauea, *J. Geophys. Res.*, *99*, 15,375–15,386, 1994.

Hill, D. P., and J. J. Zucca, Geophysical constraints on the structure of Kilauea and Mauna Loa volcanoes and some implications for seismomagmatic processes, edited by R. W. Decker, T. L. Wright, and P. H. Stauffer, *U.S. Geol. Surv. Prof. Pap. 1350*, *2*, 903–917, 1987.

Hills, D. J., J. K. Morgan, G. F. Moore, and S. C. Leslie, Structural variability along the submarine south flank of Kilauea volcano, Hawaii, from a multichannel seismic reflection survey, in *Hawaiian Volcanoes*: *Deep Underwater Perspectives*, *Geophys. Monogr. Ser.*, vol. 128, edited by E. Takahashi et al., pp. 105–124, AGU, Washington, D. C., 2002.

Holcomb, R. T., and R. C. Searle, Large landslides from oceanic volcanoes, *Mar. Geotechnol.*, *10*, 19–32, 1991.

Iverson, R. M., Can magma-injection and groundwater forces cause massive landslides on Hawaiian volcanoes?, *J. Volcanol. Geotherm. Res.*, *66*, 295–308, 1995.

Kimura, J.-I., T. Sisson, M. Coombs, and P. Lipman, In-place alkalic pillow lavas from offshore Kilauea volcano, Hawaii: Significance in reconstructing ancient Kilauea history, *Eos Trans. AGU*, *83*(47), Fall Meet. Suppl., Abstract V62B-1397, 2002.

Krastel, S., H.-U. Schmincke, C. L. Jacobs, R. Rihm, T. P. Le Bas, and B. Alibés, Submarine landslides around the Canary Islands, *J. Geophys. Res.*, *106*, 3977–3997, 2001.

Lènat, J.-F., P. Vincent, and P. Bacherley, The offshore continuation of an active basaltic volcanoe: Piton de la Fournaise (Reunion Island, Indian Ocean): Structural and geomorphological interpretation from Sea Beam mapping, *J. Volcanol. Geotherm. Res.*, *36*, 1–36, 1989.

Leslie, S. C., G. F. Moore, J. K. Morgan, and D. J. Hills, Seismic stratigraphy of the Frontal Hawaiian Moat: Implications for sedimentary processes at the leading edge of an oceanic hotspot trace, *Mar. Geol.*, *184*, 143–162, 2002.

Lipman, P. W., Declining growth of Mauna Loa during the last 100,000 years: Rates of lava accumulation vs. gravitational subsidence, in *Mauna Loa Revealed*: *Structure, Composition, History, and Hazards*, *Geophys. Monogr. Ser.*, vol. 92, edited by J. M. Rhodes and J. P. Lockwood, pp. 45–80, AGU, Washington, D. C., 1995.

Lipman, P. W., J. P. Lockwood, R. T. Okamura, D. A. Swanson, and K. M. Yamashita, Ground deformation associated with the 1975 magnitude-7.2 earthquake and resulting changes in activity of Kilauea volcano, Hawaii, *U.S. Geol. Surv. Prof. Pap., 1276*, 45 pp., 1985.

Lipman, P. W., W. R. Normark, J. G. Moore, J. B. Wilson, and C. E. Gutmacher, The giant submarine Alika debris slide, Mauna Loa, Hawaii, *J. Geophys. Res.*, *93*, 4279–4299, 1988.

Lipman, P. W., T. W. Sisson, T. Ui, J. Naka, and J. R. Smith, Ancestral submarine growth of Kilauea volcano and instability of its south flank, in *Hawaiian Volcanoes*: *Deep Underwater Perspectives*, *Geophys. Monogr. Ser.*, vol. 128, edited by E. Takahashi et al., pp. 161–191, AGU, Washington, D. C., 2002.

Ma, K.-F., H. Kanamori, and K. Satake, Mechanism of the 1975 Kalapana, Hawaii earthquake inferred from tsunami data, *J. Geophys. Res.*, *104*, 13,153–13,167, 1999.

Macdonald, G. A., and A. T. Abbott, *Volcanoes in the Sea*, Univ. of Hawaii Press, Honolulu, 1970.

MBARI Mapping Team, Hawaii Multibeam Survey, *Monterey Bay Aquarium Research Institute Digital Data Series No. 2,* 2-CD set, 2001.

McMurtry, G. M., E. Herrero-Bervera, M. D. Cremer, J. R. Smith, J. Resig, C. Sherman, and M. E. Torresan, Stratigraphic constraints on the timing and emplacement of the Alika 2 giant Hawaiian submarine landslide, *J. Volcanol. Geotherm. Res.*, *94*, 35–58, 1999.

Moore, J. G., and W. W. J. Chadwick, Offshore geology of Mauna Loa and adjacent areas, Hawaii, in *Mauna Loa Revealed*: *Structure, Composition, History, and Hazards*, *Geophys. Monogr. Ser.*, vol. 92, edited by J. M. Rhodes and J. P. Lockwood, pp. 21–44, AGU, Washington, D. C., 1995.

Moore, J. G., and R. S. Fiske, Volcanic substructure inferred from dredge samples and ocean-bottom photographs, Hawaii, *Geol. Soc. Am. Bull.*, *80*, 1191–1202, 1969.

Moore, J. G., and H. L. Krivoy, The 1962 flank eruption of Kilauea volcano and structure of the east rift zone, *J. Geophys. Res.*, *69*, 2033–2045, 1964.

Moore, J. G., and D. L. Peck, Bathymetric, topographic, and structural map of the south-central flank of Kiluea volcano, Hawaii, *U.S, Geol. Surv. Misc. Geol. Invest. Map, I-456*, 1965.

Moore, J. G., R. L. Phillips, R. W. Grigg, D. W. Peterson, and D. A. Swanson, Flow of lava into the sea, 1969–1971, Kilauea volcano, Hawaii, *Geol. Soc. Am. Bull.*, *84*, 537–546, 1973.

Moore, J. G., D. A. Clague, R. T. Holcomb, P. W. Lipman, W. R. Normark, and M. E. Torresan, Prodigious submarine landslides on the Hawaiian Ridge, *J. Geophys. Res.*, *94*, 17,465–17,484, 1989.

Moore, J. G., W. R. Normark, and R. T. Holcomb, Giant Hawaiian landslides, *Annu. Rev. Earth Planet. Sci.*, *22*, 119–144, 1994.

Morgan, J. K., and D. A. Clague, Volcanic spreading on Mauna Loa volcano, Hawaii: Evidence from accretion, alteration, and exhumation of volcaniclastic sediments, *Geology*, *30*, 411–414, 2003.

Morgan, J. K., G. F. Moore, D. J. Hills, and S. Leslie, Overthrusting and sediment accretion along Kilauea's mobile south flank, Hawaii: Evidence for volcanic spreading from marine seismic reflection data, *Geology*, *28*, 667–670, 2000.

Nakamura, K., Why do long rift zones develop better in Hawaiian volcanoes? A possible role of thick oceanic sediments, *Bull. Volcanol. Soc. Jpn.*, *25*, 255–269, 1980.

Okubo, P. G., H. M. Benz, and B. A. Chouet, Imaging the crustal magma sources beneath Mauna Loa and Kilauea volcanoes, Hawaii, *Geology*, *25*, 867–870, 1997.

Owen, S., P. Segall, J. Freymueller, A. Miklius, R. Denlinger, T. Arnadottir, M. Sako, and R. Bürgmann, Rapid deformation of the south flank of Kilauea volcano, Hawaii, *Science*, *267*, 1328–1332, 1995.

Owen, S., P. Segall, M. Lisowski, A. Miklius, R. Denlinger, and M. Sako, Rapid deformation of Kilauea volcano: Global positioning system measurements between 1990 and 1996, *J. Geophys. Res.*, *105*, 18,983–18,998, 2000.

Riley, C. M., J. F. Diehl, J. L. Kirschvink, and R. L. Ripperdan, Paleomagnetic constraints on fault motion in the Hilina fault system, south flank of Kilauea volcano, Hawaii, *J. Volcanol. Geotherm. Res.*, *94*, 233–249, 1999.

Salisbury, M. H., N. I. Christensen, and R. H. Wilkens, Nature of the layer 2/3 transition from a comparison of laboratory and logging velocities and petrology at the base of Hole 504B, *Proc. Ocean Drill. Program Sci. Results*, *148*, 409–414, 1996.

Satake, K., J. R. Smith, and K. Shinozaki, Three-dimensional reconstruction and tsunami model of the Nuuanu and Wailau giant landslides, Hawaii, in *Hawaiian Volcanoes*: *Deep Underwater Perspectives*, *Geophys. Monogr. Ser.*, vol. 128, edited by E. Takahashi et al., pp. 333–346, AGU, Washington, D. C., 2002.

Sisson, T. W., P. W. Lipman, and J. Naka, Submarine alkalic through tholeiitic shield-stage development of Kilauea volcano, Hawaii, in *Hawaiian Volcanoes*: *Deep Underwater Perspectives*, *Geophys. Monogr. Ser.*, vol. 128, edited by E. Takahashi et al., pp. 193–219, AGU, Washington, D. C., 2002.

Smith, J. R., Jr., Volcano instability on the submarine south flank of Hawaii Island, Ph.D. dissertation, Univ. of Hawaii, Honolulu, 1996.

Smith, J. R., A. N. Shor, A. Malahoff, and M. E. Torresan, Southeast flank of Island of Hawaii, SeaBeam multibeam bathymetry, HAWAII MR1 sidescan sonar imagery, and magnetic anomalies, in *Hawaii Seafloor Atlas*, scale 1:250000, sheet 4, Hawaii Inst. of Geophys. and Planetology, Honolulu, Hawaii, 1994.

Smith, J. R., A. Malahoff, and A. N. Shor, Submarine geology of the Hilina slump and morpho-structural evolution of Kilauea volcano, Hawaii, *J. Volcanol. Geotherm. Res.*, *94*, 59–88, 1999.

Stearns, H. T., and W. O. Clark, Geology and water resources of the Kau District, Hawaii, *U.S. Geol. Surv. Water Supply Pap.*, *616*, 194 pp., 1930.

Swanson, D. A., W. A. Duffield, and R. S. Fiske, Displacement of the south flank of Kilauea volcano: The result of forceful intrusion of magma into the rift zones, *U.S. Geol. Surv. Prof. Pap.*, *963*, 39 pp., 1976.

Tilling, R. I., R. Y. Koyanagi, P. W. Lipman, J. P. Lockwood, J. P. Moore, and D. A. Swanson, Earthquake and related catastrophic events, island of Hawaii, November 29, 1975: A preliminary report, *U.S. Geol. Surv. Circ.*, *740*, 33 pp., 1976.

Thurber, C. H., Seismic structure and tectonics of Kilauea volcano, edited by R. W. Decker, T. L. Wright, and P. H. Stauffer, *U.S. Geol. Surv. Prof. Pap., 1350*, *2*, 919–934, 1987.

Ward, S. N., News and views: Slip-sliding away, *Nature*, *415*, 973–974, 2002.

Watts, A. B., and D. G. Masson, A giant landslide on the north flank of Tenerife, Canary Islands, *J. Geophys. Res.*, *100*, 24,487–24,498, 1995.

Wolfe, C. J., M. K. McNutt, and R. S. Detrick, The Marquesas archipelagic apron: Seismic stratigraphy and implications for volcano growth, mass wasting, and crustal underplating, *J. Geophys. Res.*, *99*, 13,591–13,608, 1994.

Wood, H. O., On the earthquakes of 1868 in Hawaii, *Bull. Seismol. Soc. Am.*, *4*, 169–203, 1914.

Wyss, M., A proposed source model for the great Kau, Hawaii, earthquake of 1868, *Bull. Seismol. Soc. Am.*, *78*, 1450–1462, 1988.

Yilmaz, O., Seismic Data Processing, in *Investigations in Geophysics*, vol. 2, Soc. of Explor. Geophys., Tulsa, Okla., 1987.

D. A. Clague, Monterey Bay Aquarium Research Institute, 7700 Sandholdt Road, Moss Landing, CA 95039-0628, USA. (clague@mbari.org)

G. F. Moore, Department of Geology and Geophysics, SOEST, University of Hawaii, 1680 East-West Road, Honolulu, HI 96822, USA. (gmoore@hawaii.edu)

J. K. Morgan, Department of Earth Science, Rice University, 6100 Main Street, MS-126, Houston, TX 77005-1892, USA. (morganj@rice.edu)

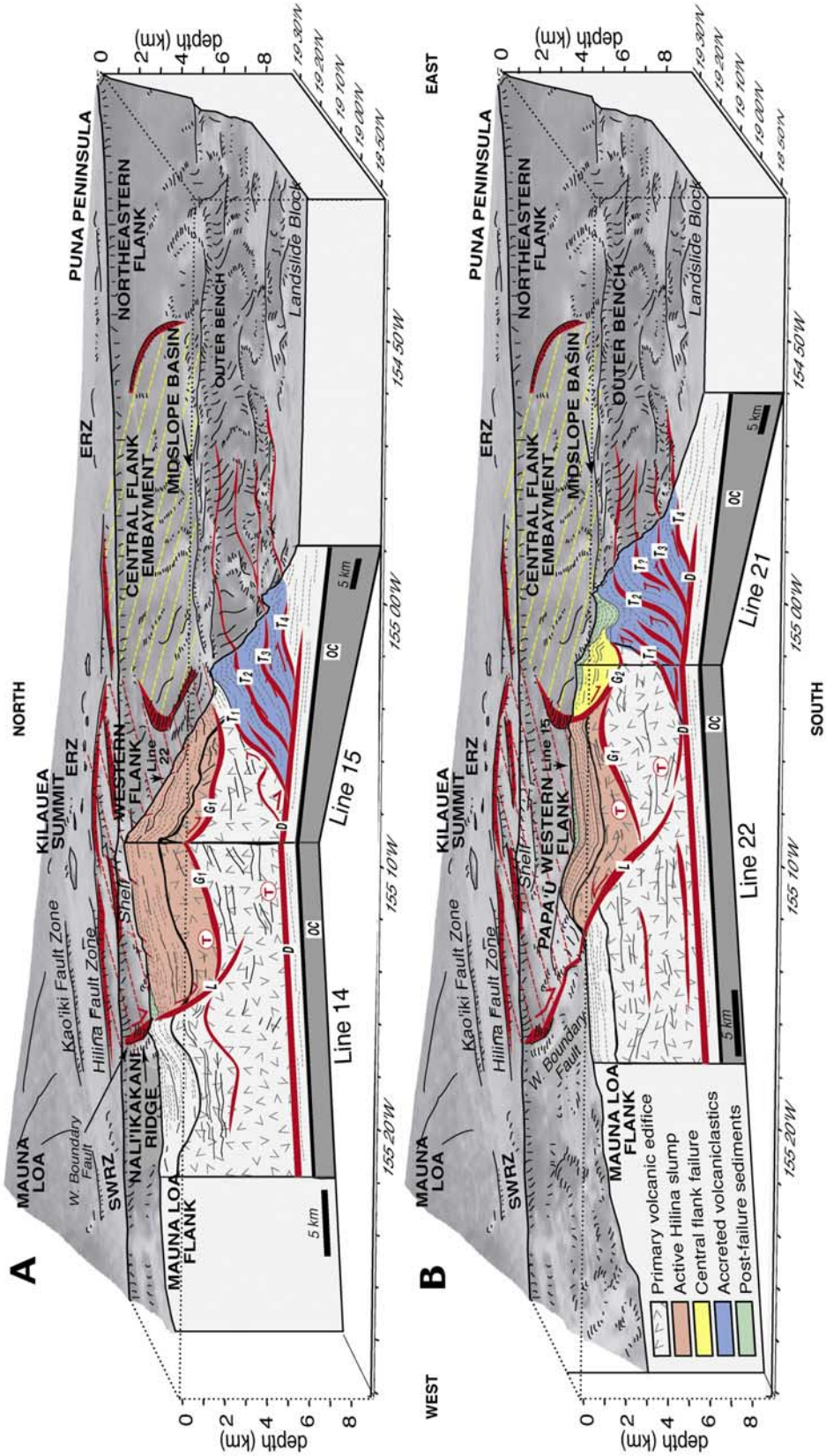

Figure 9. Cutaway views through Kilauea's south flank showing subsurface structures compiled from the seismic data. (a) Lines 14 and 15 reveal the structure of the western flank, detachment G_1, and the Hilina slump. Extension along Nali'ikakani Ridge, and folding and faulting of the shallow sediments on Line 15 result from downslope movement of the Hilina slump. Deeper structures are primarily landward dipping, accommodating thrusting and accretion of volcaniclastic strata within the outer bench. (b) Lines 22 and 21 show uplift and westward thrusting of Papa'u due to oblique convergence of the Hilina slump upon the western boundary fault. The transition to the region of central flank failure is marked an arcuate scarp at the seafloor, and listric G_2 detachment at depth. Imbricate thrust sheets within the outer bench front the central flank embayment, ponding sediments within the midslope basin.